Crucial Role of the YAP/TEAD Axis in Osteosarcoma Tumor Growth: Effects of YAP Inhibitors Verteporfin and CA3 on Tumor Growth *in vivo*

Sarah Morice
Nantes University
Mathilde Mullard
Nantes University
Regis Brion
Nantes University
Maryne Dupuy
Nantes University
Sarah Renault
Nantes University
Robel Tesfaye
Nantes University
Benjamin Ory
Nantes University
Francoise Redini
Nantes University
Franck Verrecchia (franck.verrecchia@univ-nantes.fr)
Nantes University https://orcid.org/0000-0003-4920-2554

Research

Keywords: Hippo/YAP, TEAD, tumor growth, osteosarcoma, verteporfin, CA3

Posted Date: November 24th, 2020

DOI: https://doi.org/10.21203/rs.3.rs-111013/v1

Abstract

Background

Osteosarcoma is the first primary bone tumor in children and adolescents. Despite progress in the understanding of the biology of these tumors, survival rates have progressed very little in recent decades. In this context, although some studies suggested that disruption of the Hippo signaling pathway is associated with osteosarcoma progression, the molecular mechanisms by which YAP regulates primary tumor growth is not fully clarified. In addition, the validation of YAP as a therapeutic target through the use of inhibitors in a preclinical model must be demonstrated.

Methods

The identification of a YAP signature was carried out by RNAseq analysis from a cohort of patients. Survival rates were assessed by Kaplan-Meier assays. The role of TEAD in the control of osteosarcoma cell proliferation by YAP has been realized by various molecular and cellular biology approaches (RNAseq, PLA, immunoprecipitation, promoter/specific gene, proliferation, cell cycle assays) using overexpression of mutated forms of YAP able or unable to interact with TEAD. The role of TEAD in YAP regulation of primary tumor growth, and the effects of YAP inhibitors *in vivo* were realized using an orthotopic model of osteosarcoma.

Results

RNA-seq analysis and Kaplan-Meier assays identified a YAP signature in osteosarcoma patients and a correlation with patients outcome. Molecular and cellular analysis using overexpression of mutated forms of YAP able or unable to interact with TEAD, indicate that TEAD is crucial for YAP-driven cell proliferation and *in vivo* tumor growth. In addition, *in vivo* experiments show that two YAP/TEAD inhibitors, verteporfin and CA3, reduce primary tumor growth. In this context, *in vitro* experiments demonstrate that these inhibitors decrease YAP expression, YAP/TEAD transcriptional activity and cell viability mainly by their ability to induce cell apoptosis.

Conclusion

We thus demonstrate that the YAP/TEAD signaling axis is a central actor in mediating primary tumor growth of osteosarcoma, and that the use of YAP inhibitors may be a promising therapeutic strategy against osteosarcoma tumor growth.

Background

Osteosarcoma (OS) is the most common primary malignant bone tumor in children and adolescents [1–3]. Although some predisposing genetic factors such as p*53* mutations have been identified, the exact etiology of this disease remains unknown [1, 4]. The standard treatment of OS consists of complete surgical resection associated with neo-adjuvant and adjuvant chemotherapies [5–8]. Unfortunately, OS is a particularly chemotherapy-resistant tumor [9] and resistance to treatment remains one of the main causes of death in OS patients, with a 5-year survival rate of only around 20–25% [7, 10, 11]. The lack of response to conventional treatments underscores the urgency to develop novel therapeutic strategies. In this context, advances in the understanding of the molecular basis of OS pathogenesis in parallel with the emergence of therapies developed to specifically inhibit cancer-associated signaling pathways seem to be of interest.

The highly conserved Hippo signaling pathway plays a critical role in the regulation of many cellular processes, such as cell proliferation, apoptosis, migration and differentiation [12, 13]. The intracellular factors of the canonical Hippo signaling pathway are mainly composed of mammalian Ste20-like kinases 1/2 (MST1/2), large tumor suppressor 1/2 (LATS1/2), Yes-Associated Protein (YAP) and its paralog transcriptional coactivator with PDZ-binding motif (TAZ). Following the activation of the Hippo signaling pathway, activated MST1/2 proteins phosphorylate and activate LATS1/2 factors which in turn phosphorylate YAP/TAZ factors, resulting in the inhibition of YAP/TAZ activity. When the Hippo signaling pathway is not activated, neither YAP nor TAZ is phosphorylated, and they can thus translocate into the nucleus, where they act as co-transcriptional factors [14]. The primary DNA-binding partners of YAP are TEA-domain DNA-binding transcription factor 1–4 (TEAD1-4) proteins able to regulate target genes that control essential cellular process including proliferation, differentiation and apoptosis [15]. Accumulating evidence has shown that disruption of the Hippo signaling pathway or abnormal activation of YAP/TAZ is closely associated with many diseases, including cancers [13, 16–20]. YAP/TAZ have thus been shown to be crucial for different steps of cancer development, such as cancer initiation,

progression and metastasis, and in the formation of tumors in different organs such as lung, prostate, breast, liver, stomach, pancreas and brain [21].

Concerning primary bone tumors, tissue array analyses have demonstrated a high level of YAP protein expression in OS tumor tissues compared to surrounding non-cancerous ones [22] and this YAP overexpression is associated to poor prognosis [23]. The molecular mechanisms underlying YAP overexpression in OS seem to be complex, but evidence suggests that it could be due in large part to the stem cell transcription factor SOX2 [24]. The findings of studies using knockdown approaches suggest that YAP and its transcriptional factor TEAD1 participate in the control of OS cell lines proliferation [25]. However, the molecular mechanisms by which YAP regulate tumor growth and the effects of YAP inhibitors, such as verteporfin and CA3, on *in vivo* OS tumor growth remain to be elucidated. In this context, using molecular and cellular approachs, the aims of this work were (i) to define the role of YAP in OS primary tumor growth, (ii) to elucidated the role of TEAD in YAP-driven OS tumor growth *in vivo*, and (iii) to evaluate the effects of two specific YAP-inhibitors, verteporfin and CA3, on the OS tumors growth using an orthotopic mouse model.

Methods And Materials

Osteosarcoma mouse model

Four-week-old female Rj:NMRI-nude mice (Janvier, Le Genest Saint Isle, France) were maintained under pathogen-free conditions at the Experimental Therapy Unit (Faculty of Medicine, Nantes, France) in accordance with the institutional guidelines of the French Ethical Committee (CEEA Pays de la Loire n°06 : project authorization 8405). Mice received an intramuscular injection of 1.10^6 K-HOS parental or mutant cells in close proximity to the tibia. Five days after cell injections, groups of mice received or not the molecules verteporfin (20 mg/kg), CA3 (10 mg/kg) or control vehicle twice a week by intraperitoneal injection. The tumor volume (V) was calculated from the measurement of three perpendicular diameters using a caliper according to the following formula: V = (length x height x depth)/2.

Cell culture and reagents.

K-HOS (CRL-1544), HOS-MNNG (CRL-1543), MG-63 (CRL-1427) and G292 (CRL-1423) osteosarcoma cell lines were purchased from ATCC (LGC Standards, Molsheim, France). HEK293 cells were purchased from Invitrogen (Thermo Fisher, Courtaboeuf, France). Cells were cultured in DMEM (Dulbecco's Modified Eagle's Medium, Lonza, Basel, Switzerland) supplemented with 10% fetal calf serum (Hyclone Perbio, Bezons, France).

To generate mutant YAP-S94A and YAP-S127A expressing cells, retrovirus infection was performed by transfecting 293 Phoenix retrovirus packaging cells with empty vector, pQCXIH-Myc-YAP-S94A and pQCXIH-Flag-YAP-S127A. pQCXIH-Myc-YAP-S94A and pQCXIH-Flag-YAP-S127A were gifts from Kunliang Guan (respectively Addgene plasmid #33094 and #33092; http://n2t.net/addgene:33094 and 33092; RRID:Addgene-33094 and -33092). pQCXIH CMV/TO DEST (w382-1) was a gift from Eric Campeau and Paul Kaufman (Addgene plasmid #17394; http://n2t.net/addgene:17394; RRID:Addgene-17394). 24 hours post-transfection, retroviral supernatant was supplemented with 5 µg/ml polybrene (Santa Cruz Biotechnology, CA, USA), filtered through a 0.45-µm filter and used to infect K-HOS cells. 48 hours after infection, cells were selected with 200 µg/ml hygromycin-B (Invitrogen, Courtaboeuf, France). Verteporfin and CA3 were respectively purchased from Tocris (Bristol, UK), and InvivoChem (Libertyville, IL, US)

Luciferase reporter assay and plasmid constructs

Transient cell transfections were performed with jetPEI™ (Polyplus transfection, Illkirch, France). The pRLTK-Renilla luciferase expression vector was co-transfected in all experiments to monitor transfection efficiencies. Luciferase activity was determined with the Dual-Luciferase reporter assay system (Promega, Charbonnieres, France). The 8xGTIIC-Luc (gift from Stefano Piccolo, Addgene plasmid #34615; http://n2t.net/addgene:34615; RRID:Addgene-34615, $(TEAD)_8$-lux in the text) construct was used as a specific reporter construct specific for TEAD-driven signaling.

Real time proliferation and Annexin V assays

In vitro cell proliferation assays were assessed using xCELLigence Real-Time cell-Analyzer (ACEA Biosciences, San Diego, CA). The experiment was done in triplicate and repeated three times.

Annexin V assay : OS cells were cultured and treated with or without verteporfin or CA3 for 72h. Cells undergoing apoptosis were identified by flow cytometry (Fortessa, BD Biociences, San Jose, CA) using the FITC Annexin V Apoptosis Detection Kit I (BD Biociences).

Immunofluorescence

Cells were seeded onto Ibidi µ-Slide 8 Well overnight and treated with or without verteporfin or CA3 for 48h, fixed with 4% paraformaldehyde and permeabilized with 0.5% Triton. Samples were incubated with Anti-YAP antibody (Cell signaling Technology, Leiden, The Netherlands). F-actin and nucleus were stained using respectively Alexa-fluor 488 phalloidin and DAPI. Images were acquired using a confocal microscope (NIKON A1 N-SIM) and processed using ImageJ.

RNA extraction and Real-time polymerase chain reaction

RNA was extracted from cells and tumors using NucleoSpin®RNAplus (Macherey Nagel, Duren, Germany) and reverse transcribed using the Maxima H minus first stand cDNA synthesis kit (Thermo Fisher, Courtaboeuf, France). Real-time monitoring of PCR amplification of complementary DNA was performed using DNA primers (primer sequences are available in Table 1) using QuantStudio 7 Flex Real-Time PCR System (Thermo Fisher) with SYBR® Select Master Mix (Life Technologies, Carlsbad, CA). Target gene expression was normalized to glyceraldehyde 3-phosphatedehydrogenase (GAPDH) and β-actin (ACTB) levels in respective samples as an internal standard.

Western blot analysis

Equal amounts of total protein extracts (lysis buffer: SDS 1%, Tris pH 7.4 10mM, Sodium orthovanadate 1 mM). were separated by SDS-polyacrylamide gel electrophoresis (SDS-PAGE) and transferred to PVDF Transfer membrane (Thermo Scientific, Illkirch, France). Antibodies used for western blotting were YAP1 (Proteintech, Manchester, UK), anti-Flag (Sigma Aldrich), HA-tag (Cell signaling), β-actin (Cell signaling), anti-mouse IgG-HRP (Santa Cruz Biotechnology, CA), anti-rabbit IgG-HRP (Santa Cruz). Antibody binding was visualized with the enhanced chemiluminescence system (SuperSignal West Pico Chemiluminescent Substrate, Thermo Scientific, Illkirch, France). For quantification, luminescence was detected with a Charge Couple Device (CCD) camera and analyzed using the GeneTools program (Syngene, Cambridge, United Kingdom).

Immunoprecipitation

HEK239FT cells were transfected with different vectors: pPGS-3HA-TEAD1, pCMV-Flag-YAP-S94A and pCMV-Flag-S127A-YAP were gifts from Kunliang Guan (Addgene plasmids #33055, #33102 and #27370; RRID: Addgene-33055, -33102 and -27370).

24 hours after transfection, media were changed with fresh DMEM containing 1% FCS for 24 hours. Transfected cells were then rinsed with ice-cold PBS and lysed in IP-lysis buffer (Invitrogen, Courtaboeuf, France). Equal amounts of proteins were precleared overnight at 4 °C using Protein-A/G-agarose (Santa Cruz Biotechnology, CA). Supernatants were incubated with primary antibody against Flag (Sigma Aldrich) and HA-tag (Cell signaling), for 2 h at 4 °C. 50 µL of Protein-A/G-agarose was then added and incubated overnight at 4 °C. Beads were washed three times with IP-lysis buffer; thereafter, 30 µL of Laemmli buffer was added and boiled for 5 min. After centrifugation, supernatants were harvested and processed for SDS-PAGE and Western blot as described above.

In situ proximity ligation assay (PLA), immunofluorescence and confocal microscopy

Duolink PLA ®: $5x10^3$ OS cells were seeded in Ibidi µ-Slide VI 0.4. 24 later, media was changed to DMEM with 1% FBS. Cells were then fixed with 4% PFA for 15 min at room temperature and incubated overnight at 4 °C with primary antibody against YAP (Cell signaling or Santa Cruz Biotechnology), TEF-1 (Santa Cruz). In situ PLA was performed using DuoLink in Situ Reagents (Sigma-Aldrich) according to the manufacturer's instructions.

Immunofluorescence assays: cells were seeded onto Ibidi µ-Slide 8 Well overnight, fixed with 4% paraformaldehyde for 15 min and permeabilized with 0.5% Triton. Samples were incubated with Anti-Vinculin–FITC antibody (Sigma-Aldrich). F-actin and nucleus were stained using respectively Alexa-fluor 488 phalloidin and DAPI. Images were acquired using a confocal microscope (NIKON A1 N-SIM) and processed using ImageJ.

RNA-seq analysis

RNAseq analysis was performed by Active Motif (Carlsbad, CA). Differential gene expression analysis was performed using DESeq2 package. The p-values obtained were corrected for false positives by using Independent Hypothesis Weighting (package IHW) multiple testing adjustment method. Genes were considered significantly differentially expressed if log2 fold-change was over 1 or less than -1 and FDR was less than 0.05. For the differentially expressed genes, over-representation and gene set enrichment analysis (GSEA) were done using clusterProfiler package, and results were plotted using enrichPlot . GSEA was performed using GSEA software (http://software.broadinstitute.org/gsea/). Gene sets used are described in table 2.

Statistical analysis

Histogram and data are shown as mean +/- S.D. of a minimum of three independent experiments.

Statistical analyses were performed using GraphPad Prism version 6 for Windows (GraphPad Software, La Jolla, CA), www.graphpad.com. The Wilcoxon matched test was used to compare the expression levels between OS and matched normal tissue. The Mann-Whitney test was used to compare the difference between two groups. A p-value under or equal to 0.05 was considered statistically significant.

Database:

RNA sequencing data of OS patient and matched normal tissue were downloaded from the Gene Expression Omnibus database (GSE99671, https://www.ncbi.nlm.nih.gov/geo/query/acc.cgi?acc=GSE99671).

Kaplan Meier analysis of osteosarcoma patient tumor samples was performed using the R2 Genomics Analysis and Visualization Platform. Genome-wide gene expression analyses of high-grade osteosarcoma are from GSE42352 (https://www.ncbi.nlm.nih.gov/geo/query/acc.cgi?acc=GSE42352).

Results

The elevation of Hippo target genes expression in OS patients is associated with the overall survival of patients.

To resolve outstanding questions regarding the role of the Hippo signaling pathway in OS development, we attempted to identify for a hypothetical Hippo signature in OS patients, using publicly available databases. Gene set enrichment analysis (GSEA) of expression data obtained by using RNAseq assays from a cohort of OS patients reveals a Hippo conserved signature in OS samples as compared to normal bone samples from the same patient (Figure 1A, Human Osteosarcoma *vs.* Matched normal tissue, and Figure 1B), suggesting a hyperactivity of the Hippo signaling pathway in OS patients. Indeed, multiple Hippo-regulated genes are significantly overexpressed in OS compared with normal bone tissue. These genes include, for example, *CYR61*, *THBS1*, *PAI-1*, and *BIRC5*, previously described as YAP target genes in tumor tissues (Figure 1A and Figure S1). Consistently, YAP is overexpressed in OS samples compared with normal tissue from the same patient (Figure 1C). Interestingly, high YAP transcripts significantly correlate with poor survival outcome in OS patients as illustrated in the Kaplan-Meier plot in Figure 1D

Taken together, these results highlight that the Hippo/YAP signature correlates with a poor survival outcome in OS patients.

YAP/TEAD interactions are crucial to promote YAP-driven TEAD transcriptional activity in OS cells

Since some previous studies indicated that activation of the Hippo/YAP signaling pathway induces tumor progression through the recruitment of YAP to DNA by the TEAD transcription factor family, we began our analysis by examining the relationship between YAP and TEAD in a panel of three human OS cell lines: HOS, MG63 and G292 cells. In situ PLA assays clearly demonstrate that YAP and TEAD interact (proteins localized within 40 nm of each other) in the nucleus of OS cell lines (Figure 2A and Figure S2A). To elucidate the role of TEAD in YAP-driven OS development, we then probed the consequences of YAP activation able or unable to interact with TEAD, using overexpression of either YAPS127A (constitutively active, TEAD-binding YAP protein) or YAPS94A (TEAD-binding deficient YAP protein). We first verified the expression and functionality of these mutated YAP expression vectors in transient transfection assays. As anticipated, unlike YAPS127A, YAPS94A proteins are unable to bind TEAD1 (Figure 2B) and do not induce a transcriptional response in OS cells (Figure 2C and Figure S2B). Using retroviral infection, we then established K-HOS clones stably overexpressing YAPS127A, YAPS94A or empty vector. As shown in Figure 2D, YAPS94A- and YAPS127A-transfected cells express high levels of YAP mRNA (left panel) and YAP protein (right panel). In situ PLA assays demonstrate increased YAP-TEAD interactions in the nucleus of K-HOS cells in YAPS127A cells compared to YAPS94A- or mock-transfected cells (Figure 2E). In addition, unlike YAPS94A- and mock-

transfected cells, YAPS127A cells exhibit an increased-TEAD transcriptional response as measured by luciferase reporter gene assay with the TEAD-specific reporter construct $(TEAD)_8$-lux (Figure 2F).

Taken together these results highlight that YAP/TEAD interactions are crucial in the ability of YAP to drive transcriptional activity in OS cells.

OS cell proliferation and *in vivo* OS tumor growth critically depend on YAP-TEAD interactions

Using these OS cellular tools, we then examined the functional role of TEAD in YAP-driven OS cell proliferation and *in vivo* tumor growth (Figure 3A). Real-time proliferation assays demonstrate an increase of OS cell proliferation when YAPS127A is overexpressed compared with the ability of OS cells to proliferate when YAPS94A or an empty vector is overexpressed (Figure 3B). A preclinical experimental model of OS induced by orthotopic injection of either YAPS94A-, YAPS127A- or mock-transfected OS cells demonstrates the crucial role of TEAD in YAP-driven *in vivo* OS tumor growth (Figure 3C). Indeed, 29 days after cell injection, the tumor volume is significantly increased when TEAD-interacting YAP is overexpressed (YAPS127A cells versus mock-transfected cells and YAPS127A cells versus YAPS94A cells) (Figure 3C). In contrast, the tumor volume is significantly reduced when TEAD-binding deficient YAP is overexpressed (YAPS94A- versus mock-transfected cells and YAPS94A- versus YAPS127A-transfected cells). Specifically, the mean tumor size at day 29 was 1043 ± 333 mm3 in the control group (mock-transfected cells), 1517 ± 330 mm3 when TEAD-interacting YAP is overexpressed (YAPS127A cells), and only 599 ± 140 mm3 when TEAD-binding deficient YAP is overexpressed (Figure 3C).

Taken together, these results demonstrate the crucial role of TEAD in YAP-driven cell proliferation and *in vivo* tumor growth in OS preclinical models.

Role of TEAD in YAP-driven cell cycle genes expression

To gain more insights into the crucial role of TEAD in YAP-driven cell proliferation and tumor growth, we then compared the RNA sequencing transcriptional profiles of YAPS127A-, YAPS94A- and mock-transfected cells. As shown in Figure S3, mock-, YAPS94A- and YAPS127A-transfected cells display distinct transcriptional profiles, with multiple genes significantly differentially expressed. Transcriptional analysis thus identifies 1,617 genes whose expression is regulated by the overexpression of the YAP mutated proteins able to bind TEAD (YAPS127A) or not (YAPS94A). Of these, 559 genes require the interaction between YAP and TEAD (Figure 4A). RNA-seq analysis identifies 128 genes related to positive regulation of cell proliferation (Figure 4B) that are significantly overexpressed in YAPS127A cells (compared to mock- or YAPS94A-transfected cells). These include genes directly involved in the control of cell cycle, such as *CDC25B,* and cell proliferation, such as *Gli1* or *AKT* (Figure 4B, right panel). In contrast, in YAPS94A cells, the expression of some genes related to inhibition of cell proliferation is increased, such as *CDKN1A, CDKN1C, CDKN2D* and *LATS1* (Figure 4B, right panel). Interestingly, quantitative PCR analysis indicates that the expression of *gli1* and *AKT* genes by tumor cells from mice biopsies and from cultured cells are upregulated when YAP able to interact with TEAD is over-expressed (Figures 4C and 4D). In addition, GSEA analysis indicates that overexpression of YAP-S127A increase the expression of genes involved on positive regulation of cell cycle G1-S phase transition (Figure 4E). This strongly demonstrates the crucial role of TEAD in YAP-driven gene expression, which is implicated in the regulation of both OS cell proliferation and *in vivo* tumor growth. Finally, to investigate the clinical importance of the role played by TEAD in OS tumor development, we analyzed TEAD gene expression using data extracted from the GSE99671 database [26]. Analysis of OS RNAseq data demonstrates that TEAD is overexpressed in OS biopsies compared with control samples from the same patient (Figure 4F).

Taken together, these results demonstrate: a) the crucial role of TEAD in YAP-driven cell cycle genes expression, and b) that TEAD is overexpressed in OS samples compared with normal tissue from the same patient.

Verteporfin and CA3 inhibit OS primary bone tumor.

To validate YAP/TEAD signaling as a potential therapeutic target for OS treatment, we evaluated the effect of verteporfin and CA3, two Hippo/YAP inhibitors, on primary tumor growth in a preclinical model of OS.

We first validated that verteporfin and CA3 block the YAP/TEAD cascade, as they inhibit transactivation of the TEAD-specific reporter construct $(TEAD)_8$-lux (Figures 5A) and the expression of *CYR61* (Figures 5B) or *CTGF* (Figure S4A) two target genes of the YAP/TEAD cascade. In situ PLA assays clearly demonstrate that YAP and TEAD interactions is significantly reduced when the cells are treated with verteporfin or CA3 (Figure 5C and Figure S4B). To elucidate the mechanism underlying the effect of verteporfin and CA3 on

YAP/TEAD transcriptional activity, we then evaluated the expression of YAP by immunofluorescence. A shown in Figure 5D and S4C, verteporfin and CA3 reduce the expression of YAP. These results, confirmed by Western-Blot analysis (Figure 5E and S4D) suggest that verteporfin and CA3 reduce TEAD transcriptional activity mainly by their ability to reduce YAP expression and thus YAP/TEAD interaction.

Importantly, experiments using an orthotopic preclinical model of OS demonstrate that injection of verteporfin or CA3 inhibit the OS tumor growth *in vivo* (Figures 6A). Indeed, respectively 30 and 33 days after tumor cell injection, the bone tumor volume is significantly decreased in mice treated with verteporfin or CA3. Regarding verteporfin experiments, the mean tumor size at day 30 was 2122 ± 618 mm3 when the mice were treated with vehicle (control group) and only 1258 ± 334 mm3 when the mice were treated with 20 mg/kg of verteporfin (Figure 6A, right and upper panel). Regarding CA3 experiments, the mean tumor size at day 33 was 2123 ± 535 mm3 when the mice were treated with vehicle (control group) and only 1179 ± 319 mm3 when the mice were treated with 10 mg/kg of CA3 (Figure 6A, right and lower panel). *In vitro* assays demonstrate that verteporfin and CA3 affect the cell viability of the three OS cell lines used; HOS, G292, and MG63, in a dose-dependent manners (Figures 6B). Flow cytometric Annexin V/PI assay showed that verteporfin and CA3 induce early and late apoptotic events, and cell death (Figure 6C and S5). For example, the percentage of HOS cells in early apoptosis (Annexin V+/PI-) was 3.2 ± 0.6% in the absence of drug, and was 2.1 ± 0.1% and 31.6 ± 2.8% after 72h treatment of cells with verteporfin and CA3, respectively. The percentage of HOS cells in late apoptosis (Annexin V+/PI-) was 3.9 ± 0.7% in the absence of drug, and reached 17.9 ± 7.1% and 18.7 ± 6.9% after 72h treatment of cells with verteporfin and CA3, respectively. The percentage of HOS death cells was 0.2 ± 0.1% in the absence of drug, and reached 23.7 ± 4.4% and 2.3 ± 0.3% after 72h treatment of cells with verteporfin and CA3, respectively.

Together, these results demonstrate that verteporfin and CA3 i) inhibit TEAD transcriptional activity mainly via their ability to reduce YAP expression and thus YAP/TEAD interactions, ii) inhibit *in vitro* OS cell lines viability, iii) reduce *in vivo* primary tumor growth and iv) suggest that these later effects are mainly due to their ability to induce cell apoptosis.

Discussion

The lack of response to drugs is a major obstacle to the effectiveness of treatment against OS. Although chemotherapy significantly improved the prognosis of patients with osteosarcoma after the introduction of neoadjuvant therapy in the early 1980s [27], the results have not improved since then and are approximately 70% for 5-year survival. The remaining 30% of patients have resistance to several types of chemotherapy. In this context it seems essential to develop new approachs to improve survival.

YAP/TEAD signaling as a target therapy against primary tumor growth

High YAP expression and/or YAP activation have been described in several solid tumor types and correlated with poor prognosis [19]. It has been proposed that YAP acts as an oncogene through activation of target genes that especially promote stimulation of tumor cell proliferation [28,29]. Despite the emerging importance of YAP in many cancers, the exact mechanisms driving key functions in cancer progression still remain to be resolved. While YAP expression was reported in OS, the molecular mechanisms underlying primary tumor growth have not been established in this pathology.

In this work, we first demonstrate that YAP is highly expressed in biopsies from OS patients and confirm a previous study reporting that YAP expression predicts a poor prognosis in this pathology [23]. We demonstrate the crucial role of YAP in the control of OS cell proliferation and tumor growth. Indeed, the overexpression of a constitutively active YAP (YAPS127A) promotes both the *in vitro* proliferation of OS cells and the *in vivo* growth of primary bone tumors. In several cancers, it has been demonstrated that YAP stimulates cell proliferation largely by controlling the expression of a broad number of cell cycle regulators or the expression of oncogenes, for example MYC and AP-1 family members [19]. In this work, we identify genes directly involved in the control of cell cycle, such as *CDC25B*, or involved in the regulation of oncogene expression, such as *Gli1* previously described as a pro-proliferation factor and thus as a potential therapeutic target in OS [30]. Furthermore, using overexpression of a mutant YAP protein unable to interact with TEAD1-4 (YAPS94A), we clearly demonstrate that the TEADs transcriptional factors are crucial in YAP-driven OS growth both *in vitro* and *in vivo* as previously described in other cancers [21]. Reinforcing these results, TEAD1 has been found to be highly expressed in OS patients. Together with the previous observation that TEAD1 plays a crucial role in the regulation of OS cell proliferation [25], these results strongly support the hypothesis that the YAP/TEAD axis could represent a promising target to inhibit primary OS tumor growth. Regarding the main role of TEAD transcriptional factor in the expression of YAP-driven genes, we further performed transcriptomic analysis in OS cells that identified TEAD-independent and TEAD-dependent modulation of YAP target genes in OS.

Suppression of primary tumor growth by YAP/TEAD inhibitors

To validate YAP/TEAD axis as a potential therapeutic target in OS, we evaluated the effect of two YAP inhibitors, verteporfin and CA3, on OS tumor growth [31]. Verteporfin is a light-activated drug used in photodynamic therapy for the treatment of choroidal neovascular membranes [32]. CA3 is a novel YAP inhibitor recently selected and identified through chemical library screening [33]. We specifically demonstrate that verteporfin and CA3 inhibit primary OS tumor growth. In this context, we show that verteporfin and CA3 block *in vitro* cell proliferation and induce *in vitro* cell apoptosis. In accordance with our results, verteporfin was subsequently reported to inhibit the growth of malignant cells without light activation, such as in human glioma [34]. CA3 was seen to strongly inhibits esophageal adenocarcinoma cell growth *in vitro* and exerts antitumor activity in xenograft model [33]. Both inhibitors suppress mesothelioma cancer stem cell phenotype and tumor formation [35]. Initially described as a YAP/TEAD interaction inhibitor [32], verteporfin was recently described as able to induce the degradation of YAP protein, demonstrating its capacity to target the YAP cascade via different modes of action [35,36]. Here we demonstrate that verteporfin reduces YAP expression and thus YAP-driven TEAD transcriptional activity in OS cell lines. We cannot exclude that verteporfin also inhibit YAP/TEAD direct interaction and therefore YAP/TEAD transcriptional response [37]. Regarding CA3, as previously described in only one recent work using mesothelioma cells, we demonstrated that CA3 induce the decrease of YAP production in OS cell lines [35]. Whatever the mechanisms of action, our work clearly shows that treatment with verteporfin or CA3 reduce YAP/TEAD signaling in OS cells as demonstrated using specific TEAD promoter/gene reporter assays. In addition, we have shown that verteporfin and CA3 induce cell death by apoptosis in the three cell lines tested, and therefore induce OS cell death and thus inhibits the tumor growth *in vivo*. These finding are in accordance with previous observations using cultured tumor cells in that verteporfin or CA3 induce apoptosis of tumor cells [35,38].

Conclusion

Our data clearly demonstrated that i) the Hippo/YAP signature correlates with a poor survival outcome in OS patients, ii) the crucial role of TEAD in YAP-driven cell proliferation and *in vivo* tumor growth in OS, and iii) Verteporfin and CA3, two YAP/TEAD transcriptional inhibitors, significantly reduce *in vivo* primary tumor growth mainly due to their ability to induce cell apoptosis.

In this context, this work forms the basis for the development of better approaches to improve the survival of osteosarcoma patients by identifying the YAP/TEAD axis as a promising therapeutic target. In addition, we demonstrated that YAP/TEAD transcriptional inhibitors, such as verteporfin and CA3, represent promising therapeutic drugs in OS.

Abbreviations

OS: Osteosarcoma

MST1/2: Mammalian Ste20-like kinases 1/2

LATS1/2: Large tumor suppressor ½

YAP: Yes-Associated Protein

TAZ: Transcriptional coactivator with PDZ-binding motif

TEAD: TEA-domain DNA-binding transcription factor 1-4

DMEM: Dulbecco's Modified Eagle's Medium

GAPDH: Glyceraldehyde 3-phosphatedehydrogenase

ACTB: β-actin

PLA: Proximity ligation assay

GSEA: Gene set enrichment analysis

Declarations

Ethics approval and consent to participate: Nude mice were maintained under pathogen-free conditions at the Experimental Therapy Unit (Faculty of Medicine, Nantes, France) in accordance with the institutional guidelines of the French Ethical Committee (CEEA Pays de la Loire n°06 : project authorization 8405).

Consent for publication: Not applicable

Availability of data and materials: The datasets used and/or analysed during the current study are available from the corresponding author on reasonable request.

Competing interests: The authors declare that they have no competing interests.

Funding: Not applicable

Author contributions: FV and SM conceived, designed, and led the project. SM performed most of the experiments and data analysis. MM, SR, RT and RB performed and analysed parts of the experiments. MD, BO, FR participated in the design of the project and the analysis of results. FV wrote the manuscript with input from all authors. All authors have read and approved the final manuscript.

Acknowledgments : This work was supported by Imagine for Margo, Societé Française de lutte contre les cancers et les leucémies de l'enfant et de l'adolescent, l'étoile de Martin, Enfants Cancers Santé, Ligue contre le cancer (comité 44, 49 et 85). We thank Mrs. Patricia Blanc (president of Imagine for Margo association) for her generous support. We also thank the members of Cellular and Tissular Imaging Core Facility of Nantes University (MicroPICell).

References

1. Simpson E, Brown HL. Understanding osteosarcomas. JAAPA. 2018;31:15–9.
2. Ottaviani G, Jaffe N. The epidemiology of osteosarcoma. Cancer Treat Res. 2009;152:3–13.
3. Jo VY, Fletcher CDM. WHO classification of soft tissue tumours: an update based on the 2013 (4th) edition. Pathology. 2014;46:95–104.
4. Gianferante DM, Mirabello L, Savage SA. Germline and somatic genetics of osteosarcoma - connecting aetiology, biology and therapy. Nat Rev Endocrinol. 2017;13:480–91.
5. Moore DD, Luu HH. Osteosarcoma Cancer Treat Res. 2014;162:65–92.
6. Eccles SA, Welch DR. Metastasis: recent discoveries and novel treatment strategies. Lancet. 2007;369:1742–57.
7. Grünewald TG, Alonso M, Avnet S, Banito A, Burdach S, Cidre-Aranaz F, et al. Sarcoma treatment in the era of molecular medicine. EMBO Mol Med. 2020;e11131.
8. ESMO/European Sarcoma Network Working Group. Bone sarcomas: ESMO Clinical Practice Guidelines for diagnosis, treatment and follow-up. Ann Oncol. 2014;25(Suppl 3):iii113–123.
9. Harrison DJ, Geller DS, Gill JD, Lewis VO, Gorlick R. Current and future therapeutic approaches for osteosarcoma. Expert Rev Anticancer Ther. 2018;18:39–50.
10. Duchman KR, Gao Y, Miller BJ. Prognostic factors for survival in patients with high-grade osteosarcoma using the Surveillance, Epidemiology, and End Results (SEER) Program database. Cancer Epidemiol. 2015;39:593–9.
11. Gibson TM, Mostoufi-Moab S, Stratton KL, Leisenring WM, Barnea D, Chow EJ, et al. Temporal patterns in the risk of chronic health conditions in survivors of childhood cancer diagnosed 1970-99: a report from the Childhood Cancer Survivor Study cohort. Lancet Oncol. 2018;19:1590–601.
12. Misra JR, Irvine KD. The Hippo Signaling Network and Its Biological Functions. Annu Rev Genet. 2018;52:65–87.
13. Han Y. Analysis of the role of the Hippo pathway in cancer. J Transl Med. 2019;17:116.
14. Harvey KF, Pfleger CM, Hariharan IK. The Drosophila Mst ortholog, hippo, restricts growth and cell proliferation and promotes apoptosis. Cell. 2003;114:457–67.
15. Zanconato F, Forcato M, Battilana G, Azzolin L, Quaranta E, Bodega B, et al. Genome-wide association between YAP/TAZ/TEAD and AP-1 at enhancers drives oncogenic growth. Nat Cell Biol. 2015;17:1218–27.
16. Gregorieff A, Wrana JL. Hippo signalling in intestinal regeneration and cancer. Curr Opin Cell Biol. 2017;48:17–25.

17. Moroishi T, Park HW, Qin B, Chen Q, Meng Z, Plouffe SW, et al. A YAP/TAZ-induced feedback mechanism regulates Hippo pathway homeostasis. Genes Dev. 2015;29:1271–84.
18. Sanchez-Vega F, Mina M, Armenia J, Chatila WK, Luna A, La KC, et al. Oncogenic Signaling Pathways in The Cancer Genome Atlas. Cell. 2018;173:321–37.e10.
19. Zanconato F, Cordenonsi M, Piccolo S. YAP/TAZ at the Roots of Cancer. Cancer Cell. 2016;29:783–803.
20. Pan D. The hippo signaling pathway in development and cancer. Dev Cell. 2010;19:491–505.
21. Morice S, Danieau G, Rédini F, Brounais-Le-Royer B, Verrecchia F. Hippo/YAP Signaling Pathway: A Promising Therapeutic Target in Bone Paediatric Cancers? Cancers. Multidisciplinary Digital Publishing Institute; 2020;12:645.
22. Zhang Y-H, Li B, Shen L, Shen Y, Chen X-D. The role and clinical significance of YES-associated protein 1 in human osteosarcoma. Int J Immunopathol Pharmacol. 2013;26:157–67.
23. Bouvier C, Macagno N, Nguyen Q, Loundou A, Jiguet-Jiglaire C, Gentet J-C, et al. Prognostic value of the Hippo pathway transcriptional coactivators YAP/TAZ and β1-integrin in conventional osteosarcoma. Oncotarget. 2016;7:64702–10.
24. Deel MD, Li JJ, Crose LES, Linardic CM. A Review: Molecular Aberrations within Hippo Signaling in Bone and Soft-Tissue Sarcomas. Front Oncol. 2015;5:190.
25. Chai J, Xu S, Guo F. TEAD1 mediates the oncogenic activities of Hippo-YAP1 signaling in osteosarcoma. Biochem Biophys Res Commun. 2017;488:297–302.
26. Ho XD, Phung P, Le Q, Nguyen VH, Reimann V, Prans E. E, et al. Whole transcriptome analysis identifies differentially regulated networks between osteosarcoma and normal bone samples. Exp Biol Med (Maywood). 2017;242:1802–11.
27. Rosen G, Murphy ML, Huvos AG, Gutierrez M, Marcove RC. Chemotherapy, en bloc resection, and prosthetic bone replacement in the treatment of osteogenic sarcoma. Cancer. 1976;37:1–11.
28. Kim C-L, Choi S-H, Mo J-S. Role of the Hippo Pathway in Fibrosis and Cancer. Cells. 2019;8.
29. Yu F-X, Zhao B, Guan K-L. Hippo Pathway in Organ Size Control, Tissue Homeostasis, and Cancer. Cell. 2015;163:811–28.
30. Lézot F, Corre I, Morice S, Rédini F, Verrecchia F. SHH Signaling Pathway Drives Pediatric Bone Sarcoma Progression. Cells. 2020;9.
31. Elisi GM, Santucci M, D'Arca D, Lauriola A, Marverti G, Losi L, et al. Repurposing of Drugs Targeting YAP-TEAD Functions. Cancers (Basel) [Internet]. 2018 [cited 2019 Oct 25];10. Available from: https://www.ncbi.nlm.nih.gov/pmc/articles/PMC6162436/.
32. Liu-Chittenden Y, Huang B, Shim JS, Chen Q, Lee S-J, Anders RA, et al. Genetic and pharmacological disruption of the TEAD-YAP complex suppresses the oncogenic activity of YAP. Genes Dev. 2012;26:1300–5.
33. Song S, Xie M, Scott AW, Jin J, Ma L, Dong X, et al. A Novel YAP1 Inhibitor Targets CSC-Enriched Radiation-Resistant Cells and Exerts Strong Antitumor Activity in Esophageal Adenocarcinoma. Mol Cancer Ther. 2018;17:443–54.
34. Al-Moujahed A, Brodowska K, Stryjewski TP, Efstathiou NE, Vasilikos I, Cichy J, et al. Verteporfin inhibits growth of human glioma in vitro without light activation. Sci Rep. 2017;7:7602.
35. Kandasamy S, Adhikary G, Rorke EA, Friedberg JS, Mickle MB, Alexander HR, et al. The YAP1 Signaling Inhibitors, Verteporfin and CA3, Suppress the Mesothelioma Cancer Stem Cell Phenotype. Mol Cancer Res. 2020;18:343–51.
36. Wang C, Zhu X, Feng W, Yu Y, Jeong K, Guo W, et al. Verteporfin inhibits YAP function through up-regulating 14-3-3σ sequestering YAP in the cytoplasm. Am J Cancer Res. 2016;6:27–37.
37. Zucchini C, Manara MC, Cristalli C, Carrabotta M, Greco S, Pinca RS, et al. ROCK2 deprivation leads to the inhibition of tumor growth and metastatic potential in osteosarcoma cells through the modulation of YAP activity. J Exp Clin Cancer Res. 2019;38:503.
38. Sanna L, Piredda R, Marchesi I, Bordoni V, Forcales SV, Calvisi DF, et al. Verteporfin exhibits anti-proliferative activity in embryonal and alveolar rhabdomyosarcoma cell lines. Chem Biol Interact. 2019;312:108813.
39. Kuijjer ML, Peterse EFP, van den Akker BEWM, Briaire-de Bruijn IH, Serra M, Meza-Zepeda LA, et al. IR/IGF1R signaling as potential target for treatment of high-grade osteosarcoma. BMC Cancer. 2013;13:245.

Tables

Table 1. Primer sequences for quantitative RT-PCR.

Gene	Forward	Reverse
AKT1	TACGAGAAGAAGCTCAGCCC	TTGGTCAGGTGGTGTGATGG
Gli1	CCAACTCCACAGGCATACAGGAT	CACAGATTCAGGCTCACGCTTC
GAPDH	TGGGTGTGAACCATGAGAAGTATG	GGTGCAGGAGGCATTGCT
YAP1	TGACCCTCGTTTTGCCATGA	GTTGCTGCTGGTTGGAGTTG
Cyr61	CCAGTGTACAGCAGCCTGAA	GGCCGGTATTTCTTCACACTC
CTGF	AGGAGTGGGTGTGTGACGAG	CGGGACAGTTGTAATGGCAG

Table 2. Gene set enrichment analysis

Gene set	
Hippo signature	http://software.broadinstitute.org/gsea/msigdb/geneset_page.jsp?geneSetName=CORDENONSI_YAP_CONSERVED_SIGNATURE&keywords=hippo
Positive regulation of cell proliferation (GO/0008284)	http://software.broadinstitute.org/gsea/msigdb/cards/GO_POSITIVE_REGULATION_OF_CELL_PROLIFERATION
GO positive regulation of cell cycle G1-S phase transition	https://www.gsea-msigdb.org/gsea/msigdb/cards/GO_POSITIVE_REGULATION_OF_CELL_CYCLE_G1_S_PHASE_TRANSITION.html

Figures

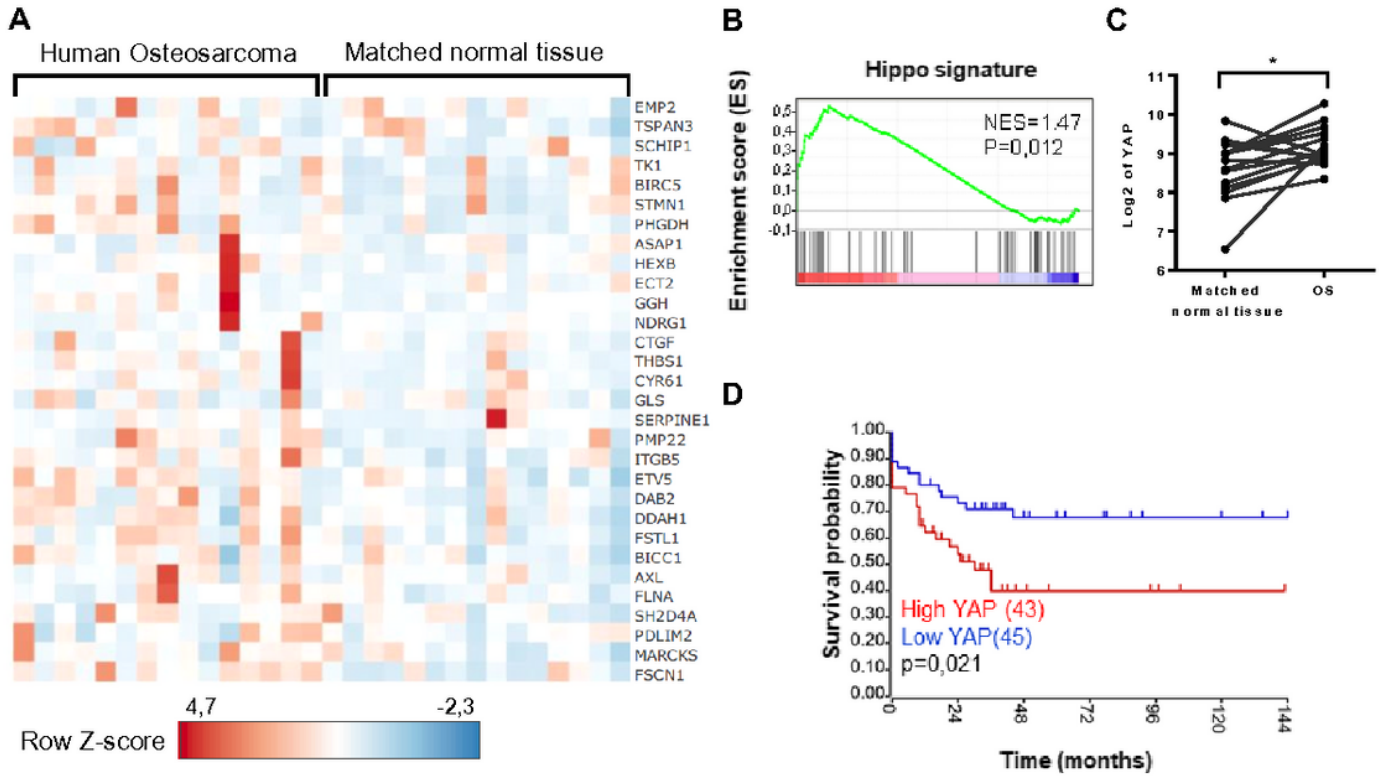

Figure 1

Elevation of Hippo gene expression in OS patients – Correlation between YAP expression and overall survival of OS patients A) Heatmap showing color-coded expression of Hippo target genes in OS tissue and matched normal tissue from the same OS patient following bioinformatics analysis of RNAseq data GSE99671 [26] from a cohort of 15 OS patients. High expression (red), low expression (blue). B) GSEA showing a Hippo signature in OS samples following bioinformatics analysis of RNAseq data GSE99671 [26] from an OS patient's cohort comprising 15 samples. FDR false discovery rate, NES normalized enrichment score. C) Relative YAP gene expression in OS samples and matched normal tissues of the same patient following bioinformatics analysis of RNAseq data GSE99671 [26]. D) Kaplan-Meier analysis of the survival outcome of patients dichotomized into high and low YAP levels, following analysis of the RNAseq dataset GSE42352 [39] from an OS patient cohort comprising 88 samples. Analysis was performed using R2 (http://r2.amc.nl). P value is from log-rank tests.

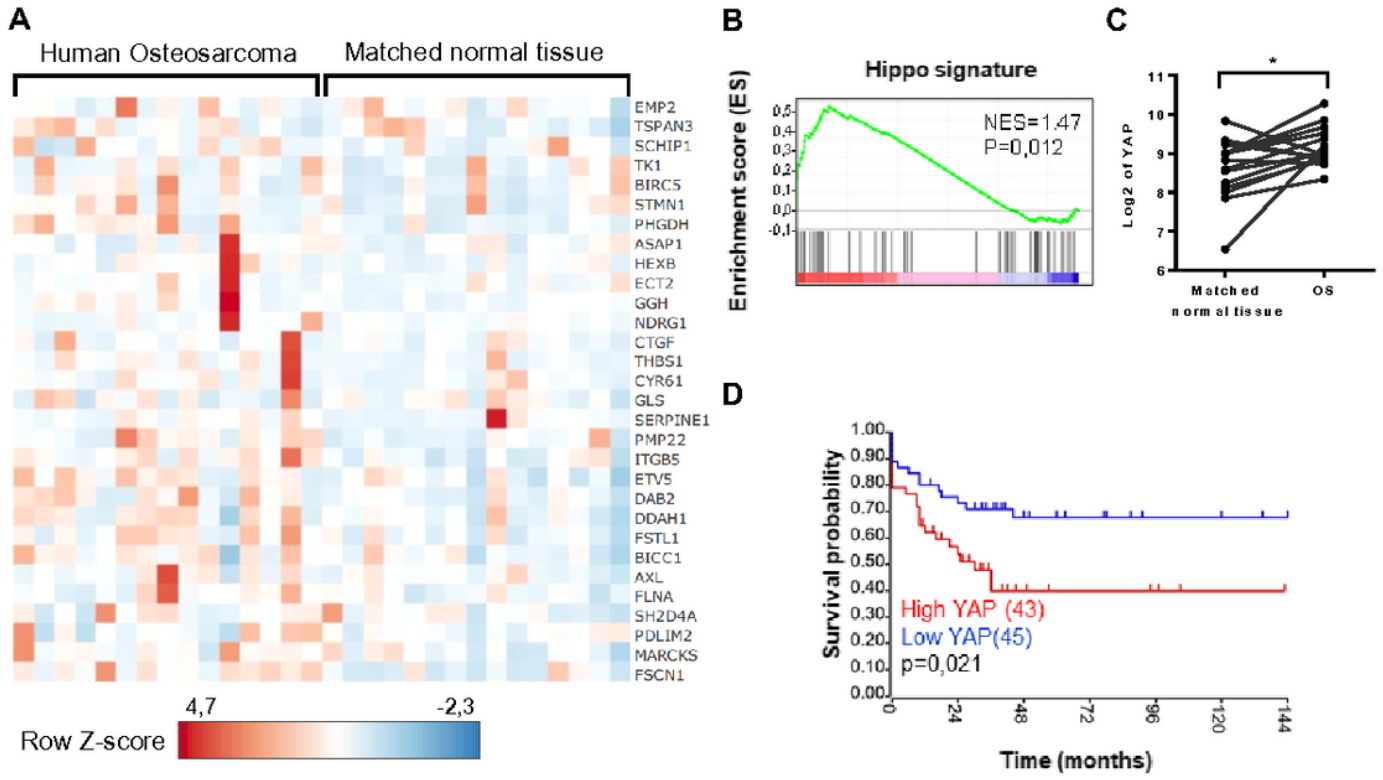

Figure 1

Elevation of Hippo gene expression in OS patients – Correlation between YAP expression and overall survival of OS patients A) Heatmap showing color-coded expression of Hippo target genes in OS tissue and matched normal tissue from the same OS patient following bioinformatics analysis of RNAseq data GSE99671 [26] from a cohort of 15 OS patients. High expression (red), low expression (blue). B) GSEA showing a Hippo signature in OS samples following bioinformatics analysis of RNAseq data GSE99671 [26] from an OS patient's cohort comprising 15 samples. FDR false discovery rate, NES normalized enrichment score. C) Relative YAP gene expression in OS samples and matched normal tissues of the same patient following bioinformatics analysis of RNAseq data GSE99671 [26]. D) Kaplan-Meier analysis of the survival outcome of patients dichotomized into high and low YAP levels, following analysis of the RNAseq dataset GSE42352 [39] from an OS patient cohort comprising 88 samples. Analysis was performed using R2 (http://r2.amc.nl). P value is from log-rank tests.

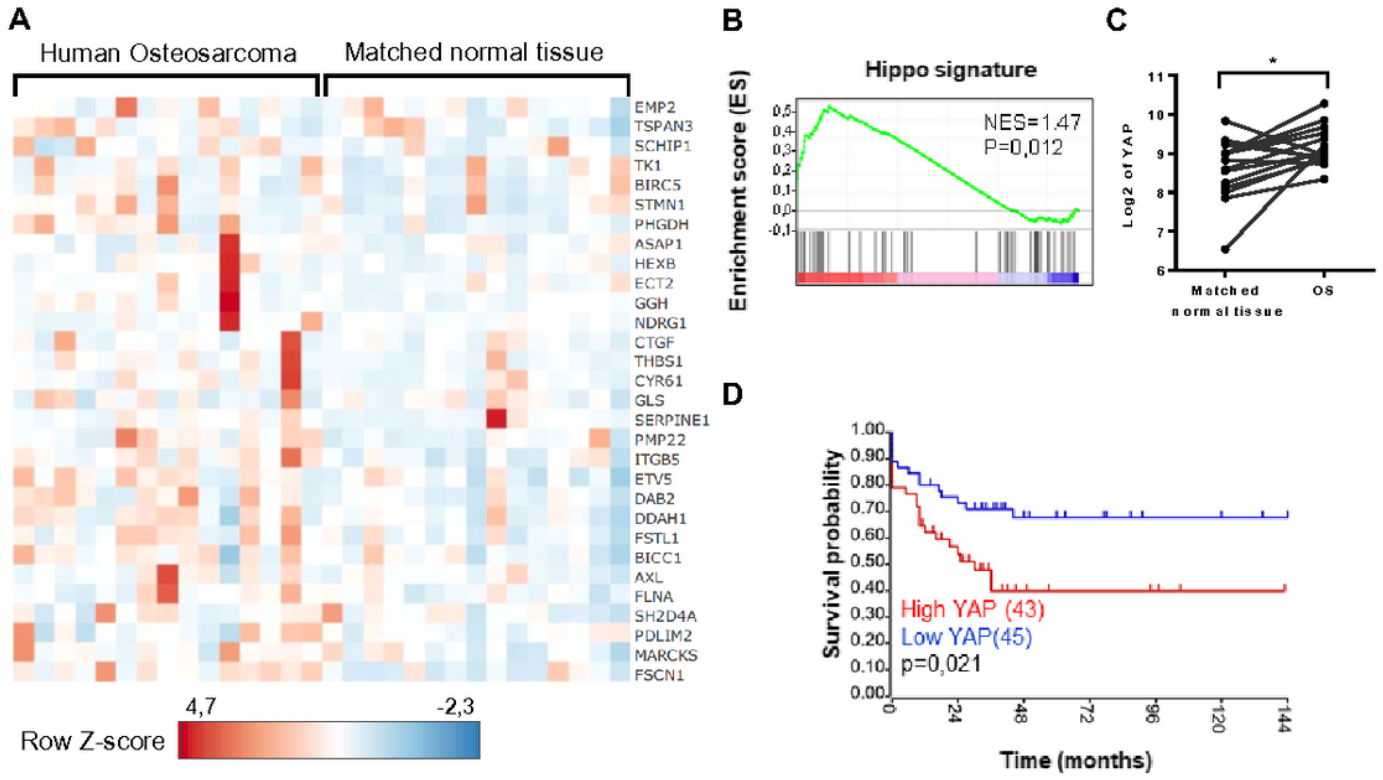

Figure 1

Elevation of Hippo gene expression in OS patients – Correlation between YAP expression and overall survival of OS patients A) Heatmap showing color-coded expression of Hippo target genes in OS tissue and matched normal tissue from the same OS patient following bioinformatics analysis of RNAseq data GSE99671 [26] from a cohort of 15 OS patients. High expression (red), low expression (blue). B) GSEA showing a Hippo signature in OS samples following bioinformatics analysis of RNAseq data GSE99671 [26] from an OS patient's cohort comprising 15 samples. FDR false discovery rate, NES normalized enrichment score. C) Relative YAP gene expression in OS samples and matched normal tissues of the same patient following bioinformatics analysis of RNAseq data GSE99671 [26]. D) Kaplan-Meier analysis of the survival outcome of patients dichotomized into high and low YAP levels, following analysis of the RNAseq dataset GSE42352 [39] from an OS patient cohort comprising 88 samples. Analysis was performed using R2 (http://r2.amc.nl). P value is from log-rank tests.

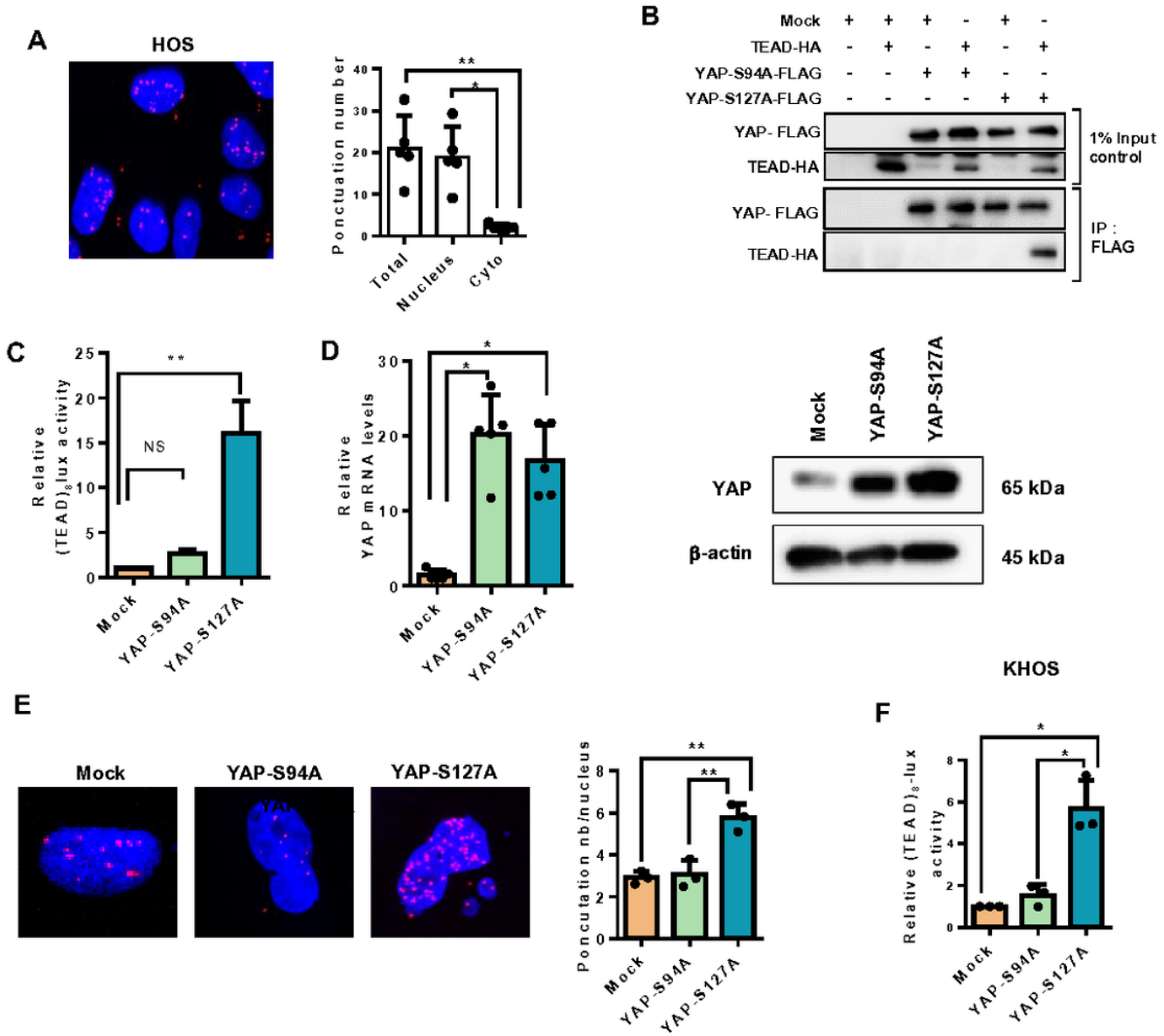

Figure 2

Role of TEAD in YAP-driven transcriptional activity A) Localization of endogenous YAP/TEAD1 complexes by in situ PLA in HOS cells. The red signal was obtained using Alexa555-labeled hybridization oligo nucleotides targeting amplified in situ PLA products. DAPI (blue) staining was used for nuclear visualization (left panel). Bars indicate means ± SD of three independent experiments (*p<0.05, **p<0.01 right panel). B) HEK293 were transiently co-transfected with the YAP-S94A, YAP-S127A, TEAD1 or empty vector as indicated. 48h after transfection lysates were subjected to immunoprecipitation (IP) with anti-Flag antibody followed by Western blotting (WB) by anti-Flag and anti-HA antibodies as indicated. C) HOS cells were co-transfected with the TEAD-specific construct (TEAD)8-lux with or without empty, YAPS94A and YAPS127A expression vectors. Bars indicate means ± SD of four independent experiments, each performed in triplicate (**p<0.01). D) YAP mRNA steady-state levels were quantified by RT-q-PCR analysis in mock-, YAPS94A- and YAPS127A-transfected K-HOS cells. Bars indicate means ± SD of four independent experiments, each performed in duplicate (*p<0.05, left panel). YAP production was detected by Western blot analysis in mock-, YAPS94A- and YAPS127A-transfected K-HOS cells. Results shown are representative of two independent experiments (right panel). E) Localization of YAP/TEAD1 complexes by in situ PLA experiments in mock-, YAPS94A- and YAPS127A-transfected K-HOS cells. The red signal was obtained using Alexa555-labeled hybridization oligo nucleotides targeting amplified in situ PLA products. DAPI (blue) staining was used for nuclear visualization (left panel). Bars indicate means ± S.D. of three independent experiments (**p<0.01, right panel). F) Mock-, YAPS94A- and YAPS127A-transfected cells were transiently transfected with the TEAD-specific construct (TEAD)8-lux. Bars indicate means ± SD of four independent experiments, each performed in duplicate (*p<0.05).

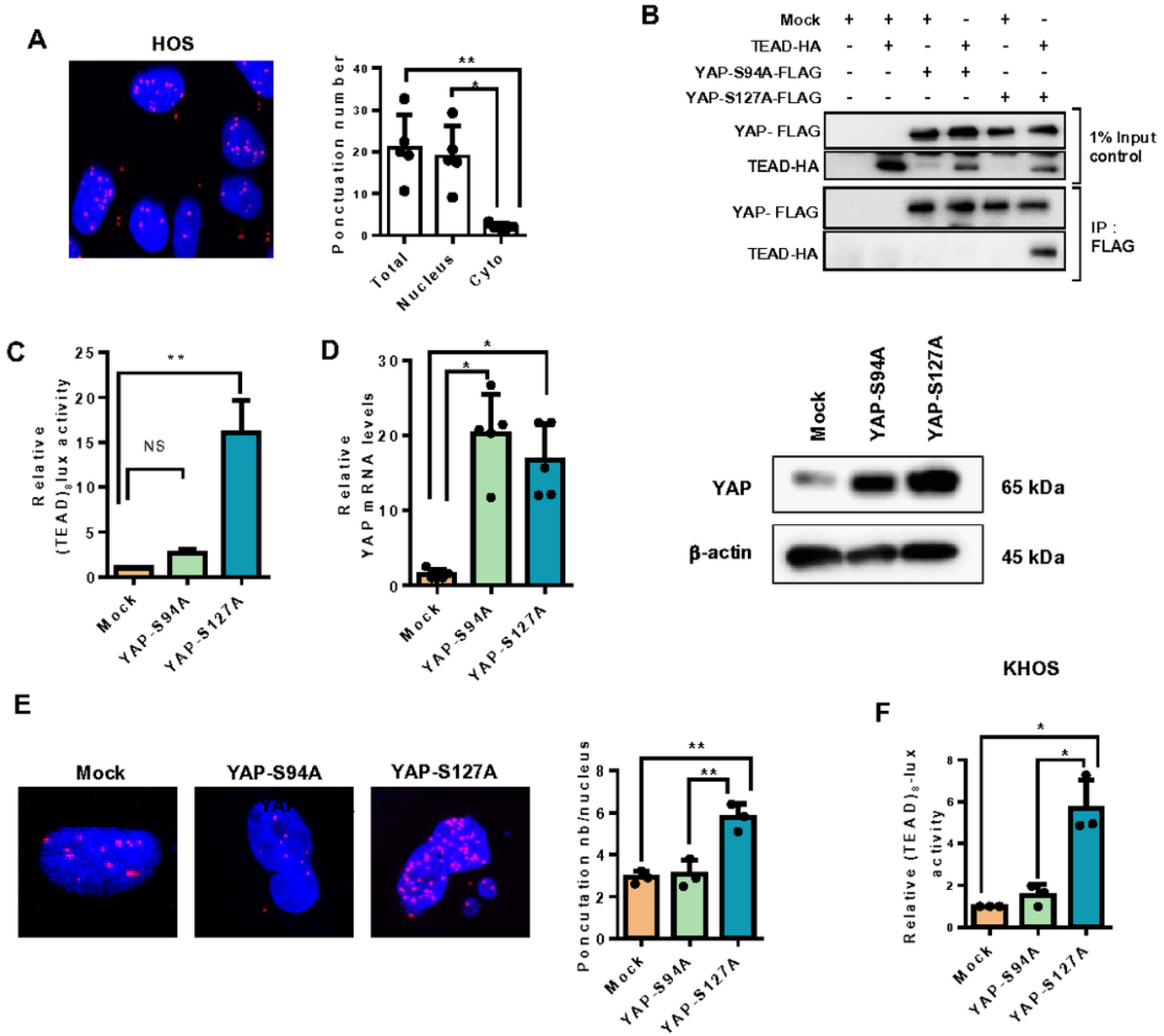

Figure 2

Role of TEAD in YAP-driven transcriptional activity A) Localization of endogenous YAP/TEAD1 complexes by in situ PLA in HOS cells. The red signal was obtained using Alexa555-labeled hybridization oligo nucleotides targeting amplified in situ PLA products. DAPI (blue) staining was used for nuclear visualization (left panel). Bars indicate means ± SD of three independent experiments (*p<0.05, **p<0.01 right panel). B) HEK293 were transiently co-transfected with the YAP-S94A, YAP-S127A, TEAD1 or empty vector as indicated. 48h after transfection lysates were subjected to immunoprecipitation (IP) with anti-Flag antibody followed by Western blotting (WB) by anti-Flag and anti-HA antibodies as indicated. C) HOS cells were co-transfected with the TEAD-specific construct (TEAD)8-lux with or without empty, YAPS94A and YAPS127A expression vectors. Bars indicate means ± SD of four independent experiments, each performed in triplicate (**p<0.01). D) YAP mRNA steady-state levels were quantified by RT-q-PCR analysis in mock-, YAPS94A- and YAPS127A-transfected K-HOS cells. Bars indicate means ± SD of four independent experiments, each performed in duplicate (*p<0.05, left panel). YAP production was detected by Western blot analysis in mock-, YAPS94A- and YAPS127A-transfected K-HOS cells. Results shown are representative of two independent experiments (right panel). E) Localization of YAP/TEAD1 complexes by in situ PLA experiments in mock-, YAPS94A- and YAPS127A-transfected K-HOS cells. The red signal was obtained using Alexa555-labeled hybridization oligo nucleotides targeting amplified in situ PLA products. DAPI (blue) staining was used for nuclear visualization (left panel). Bars indicate means ± S.D. of three independent experiments (**p<0.01, right panel). F) Mock-, YAPS94A- and YAPS127A-transfected cells were transiently transfected with the TEAD-specific construct (TEAD)8-lux. Bars indicate means ± SD of four independent experiments, each performed in duplicate (*p<0.05).

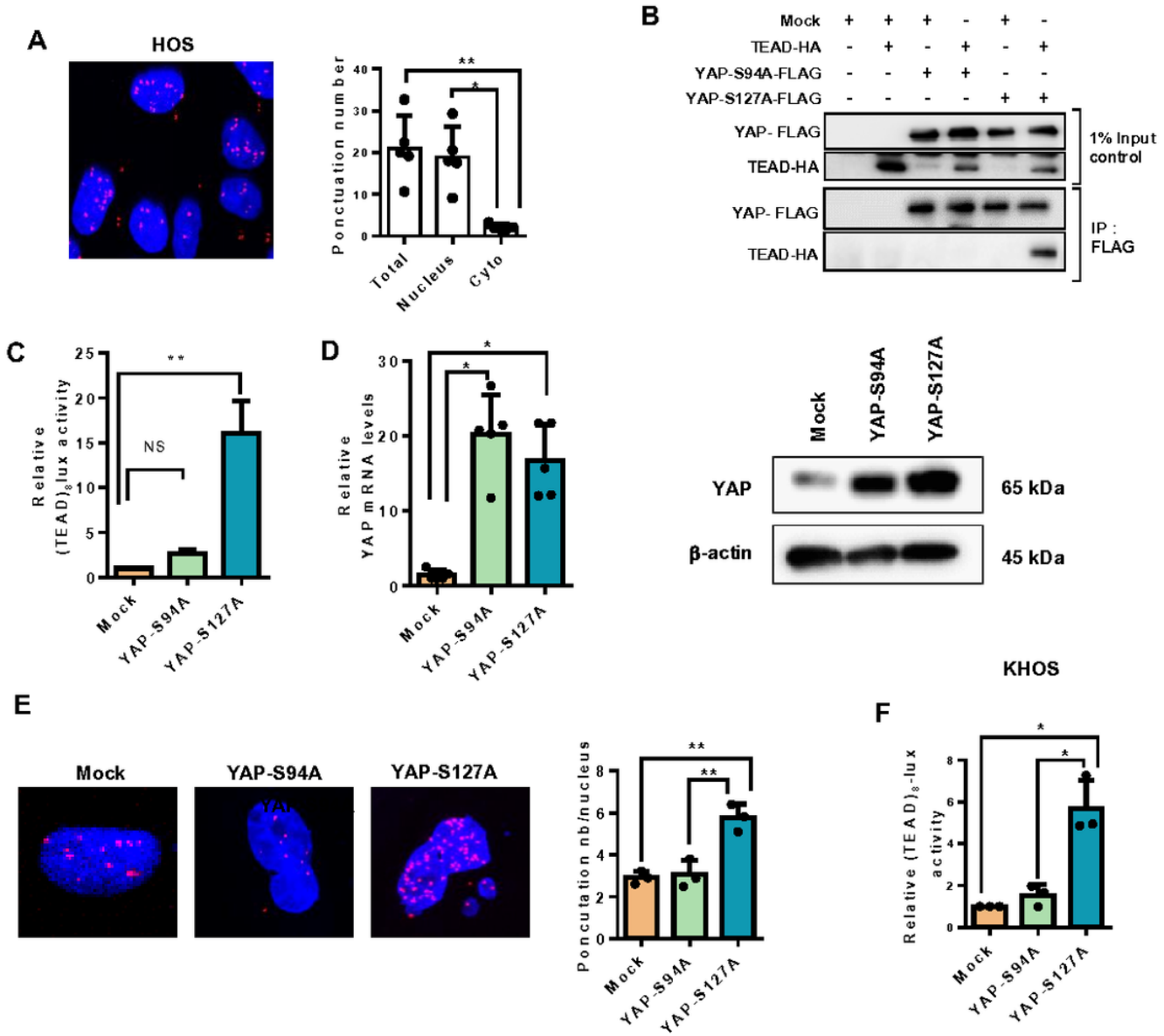

Figure 2

Role of TEAD in YAP-driven transcriptional activity A) Localization of endogenous YAP/TEAD1 complexes by in situ PLA in HOS cells. The red signal was obtained using Alexa555-labeled hybridization oligo nucleotides targeting amplified in situ PLA products. DAPI (blue) staining was used for nuclear visualization (left panel). Bars indicate means ± SD of three independent experiments (*p<0.05, **p<0.01 right panel). B) HEK293 were transiently co-transfected with the YAP-S94A, YAP-S127A, TEAD1 or empty vector as indicated. 48h after transfection lysates were subjected to immunoprecipitation (IP) with anti-Flag antibody followed by Western blotting (WB) by anti-Flag and anti-HA antibodies as indicated. C) HOS cells were co-transfected with the TEAD-specific construct (TEAD)8-lux with or without empty, YAPS94A and YAPS127A expression vectors. Bars indicate means ± SD of four independent experiments, each performed in triplicate (**p<0.01). D) YAP mRNA steady-state levels were quantified by RT-q-PCR analysis in mock-, YAPS94A- and YAPS127A-transfected K-HOS cells. Bars indicate means ± SD of four independent experiments, each performed in duplicate (*p<0.05, left panel). YAP production was detected by Western blot analysis in mock-, YAPS94A- and YAPS127A-transfected K-HOS cells. Results shown are representative of two independent experiments (right panel). E) Localization of YAP/TEAD1 complexes by in situ PLA experiments in mock-, YAPS94A- and YAPS127A-transfected K-HOS cells. The red signal was obtained using Alexa555-labeled hybridization oligo nucleotides targeting amplified in situ PLA products. DAPI (blue) staining was used for nuclear visualization (left panel). Bars indicate means ± S.D. of three independent experiments (**p<0.01, right panel). F) Mock-, YAPS94A- and YAPS127A-transfected cells were transiently transfected with the TEAD-specific construct (TEAD)8-lux. Bars indicate means ± SD of four independent experiments, each performed in duplicate (*p<0.05).

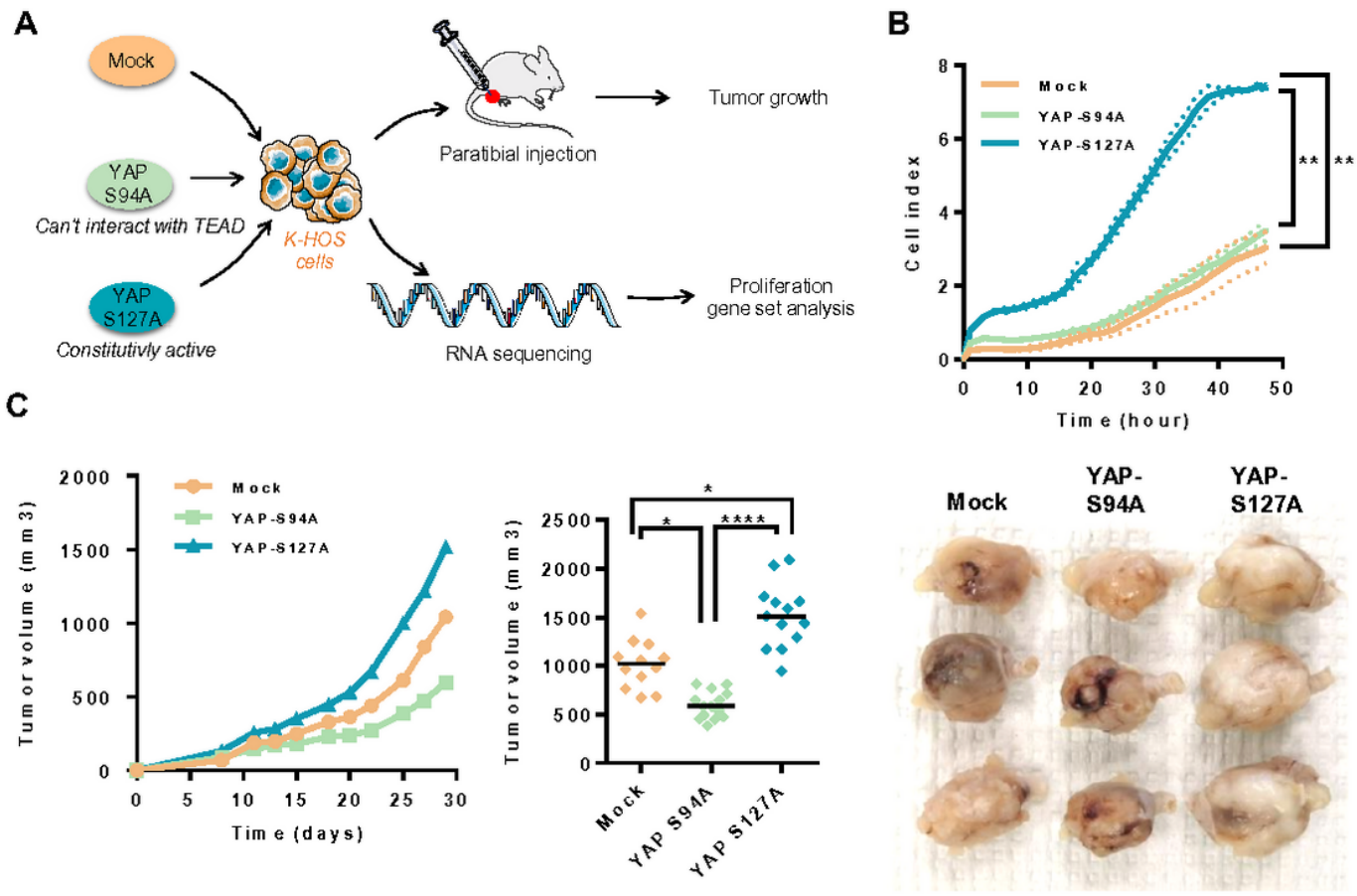

Figure 3

Role of TEAD in YAP-driven OS cell proliferation and in vivo OS tumor growth A) Schematic representation of the experimental protocols. Briefly, K-HOS cells were stably transfected with mock-, YAPS94A- or YAPS127A-vectors. Intramuscular paratibial injections of these cells were performed in nude mice, and the tumor volume was measured three time per week. In parallel, RNAseq analysis was performed on cells. B) Realtime proliferation assays were performed to compare the cell proliferation rate between mock-, YAPS94A- and YAPS127A-transfected K-HOS. Each point indicates means ± SD of three independent experiments, each performed in sextuplicate (**p<0.01). C) Intramuscular paratibial injections of 1.106 mock-, YAPS94A- and YAPS127A-transfected K-HOS cells were performed in three groups of 12 nude mice. Tumor volumes were measured three times per week for 4 weeks (left panel). Means tumor volumes of each group were measured 29 days after cell injection (middle panel, mean ± SD; *p < 0.05, ****p<0.001). Photographs show three representative bone tumors in each group of mice (right panel).

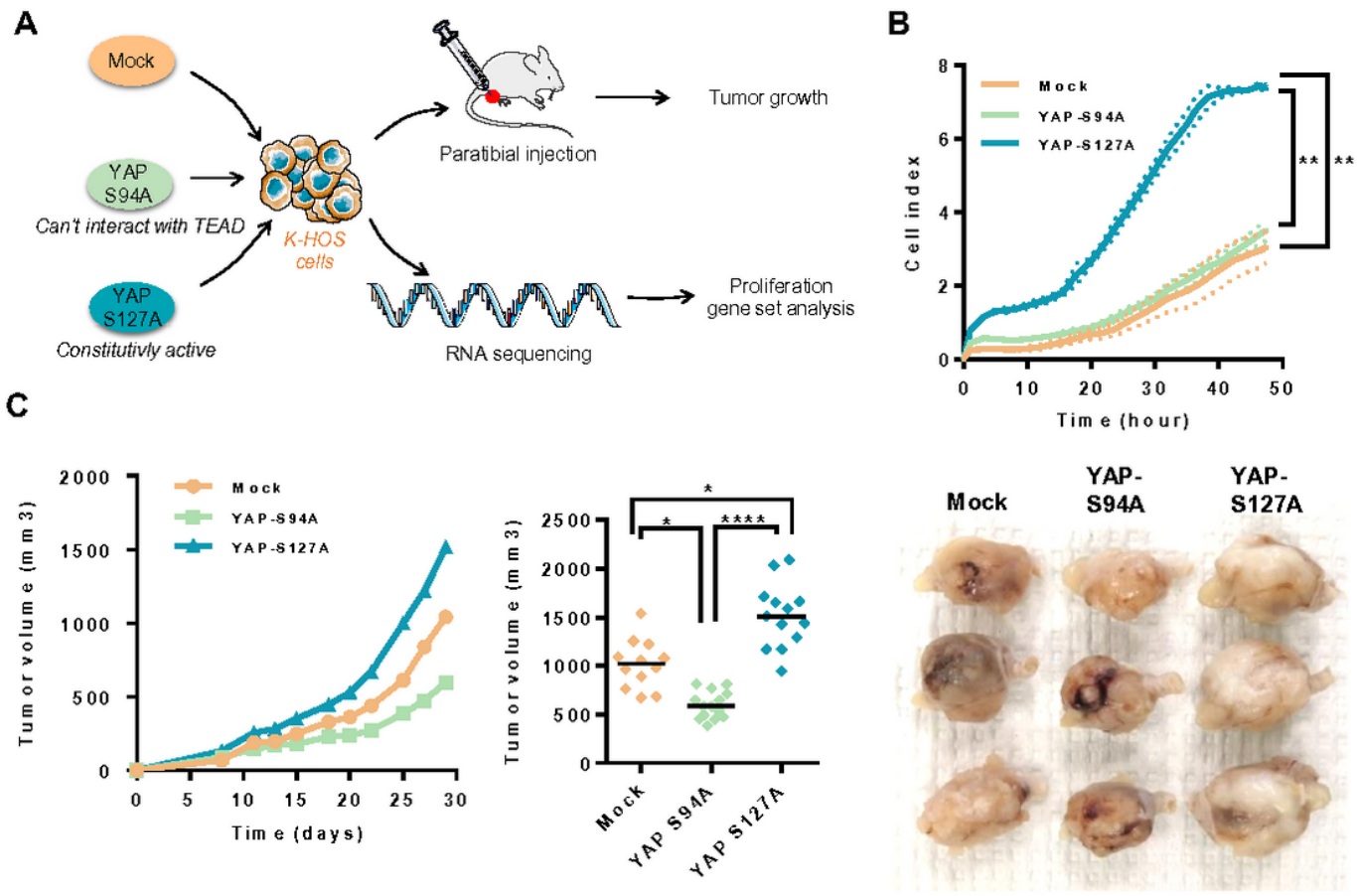

Figure 3

Role of TEAD in YAP-driven OS cell proliferation and in vivo OS tumor growth A) Schematic representation of the experimental protocols. Briefly, K-HOS cells were stably transfected with mock-, YAPS94A- or YAPS127A-vectors. Intramuscular paratibial injections of these cells were performed in nude mice, and the tumor volume was measured three time per week. In parallel, RNAseq analysis was performed on cells. B) Realtime proliferation assays were performed to compare the cell proliferation rate between mock-, YAPS94A- and YAPS127A-transfected K-HOS. Each point indicates means ± SD of three independent experiments, each performed in sextuplicate (**p<0.01). C) Intramuscular paratibial injections of 1.106 mock-, YAPS94A- and YAPS127A-transfected K-HOS cells were performed in three groups of 12 nude mice. Tumor volumes were measured three times per week for 4 weeks (left panel). Means tumor volumes of each group were measured 29 days after cell injection (middle panel, mean ± SD; *p < 0.05, ****p<0.001). Photographs show three representative bone tumors in each group of mice (right panel).

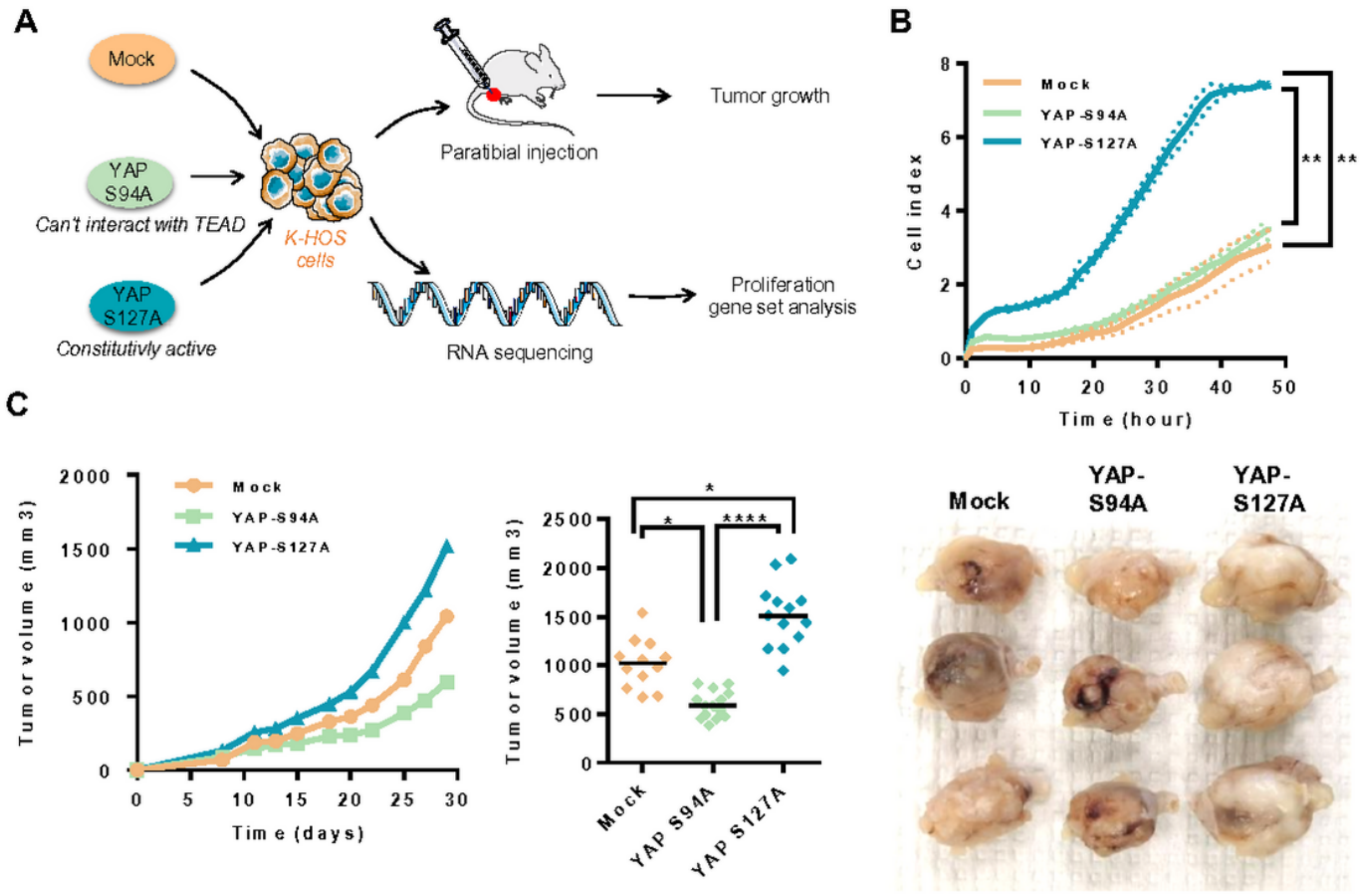

Figure 3

Role of TEAD in YAP-driven OS cell proliferation and in vivo OS tumor growth A) Schematic representation of the experimental protocols. Briefly, K-HOS cells were stably transfected with mock-, YAPS94A- or YAPS127A-vectors. Intramuscular paratibial injections of these cells were performed in nude mice, and the tumor volume was measured three time per week. In parallel, RNAseq analysis was performed on cells. B) Realtime proliferation assays were performed to compare the cell proliferation rate between mock-, YAPS94A- and YAPS127A-transfected K-HOS. Each point indicates means ± SD of three independent experiments, each performed in sextuplicate (**p<0.01). C) Intramuscular paratibial injections of 1.106 mock-, YAPS94A- and YAPS127A-transfected K-HOS cells were performed in three groups of 12 nude mice. Tumor volumes were measured three times per week for 4 weeks (left panel). Means tumor volumes of each group were measured 29 days after cell injection (middle panel, mean ± SD; *p < 0.05, ****p<0.001). Photographs show three representative bone tumors in each group of mice (right panel).

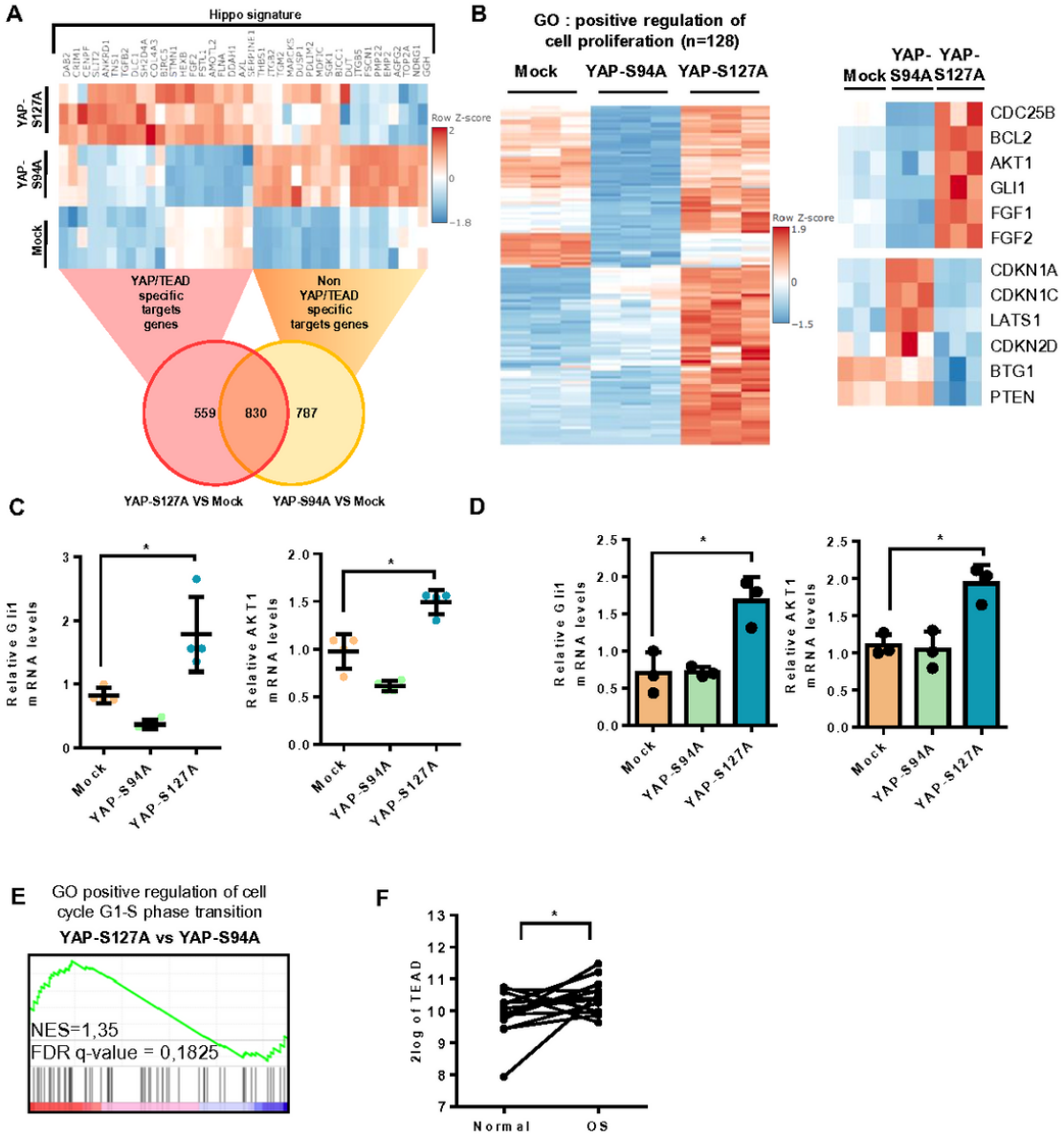

Figure 4

Role of TEAD in YAP-driven cell cycle genes expression A) Heat map of YAP-associated upregulated gene signature in mock-, YAPS94A- and YAPS127A-transfected K-HOS cells. Color scales are based on Z-scores. B) Heat map showing mRNA levels of 128 genes significantly overexpressed in YAPS127A-transfected cells involved in the positive regulation of cell proliferation. Color scales are based on Z-scores. C) Total RNA was extracted from tumor biopsies of mice injected with mock-, YAPS94A- or YAPS127A-transfected cells. Gli1 and AKT1 mRNA steady-state levels were determined by quantitative RT-PCR. Bars indicate means ± S.D. of three independent experiments, each performed in duplicate. (*p<0.05). D) Gli1 and AKT1 mRNA steady-state levels were quantified by RT-qPCR analysis in mock-, YAPS94A- and YAPS127A-transfected K-HOS cells. Bars indicate means ± SD of three independent experiments, each performed in triplicate (*p<0.05). E) Enrichment score (ES) plots of GSEA analysis show a significant upregulation of genes involved in G1-S phase transition in YAPS127A-transfected K-HOS cells compared to YAPS94A-transfected K-HOS cells. F) Relative TEAD1 gene expression in OS patients and control samples of the same patients following bioinformatics analysis of RNAseq data GSE99671 [26] from an OS patient cohort comprising 15 samples.

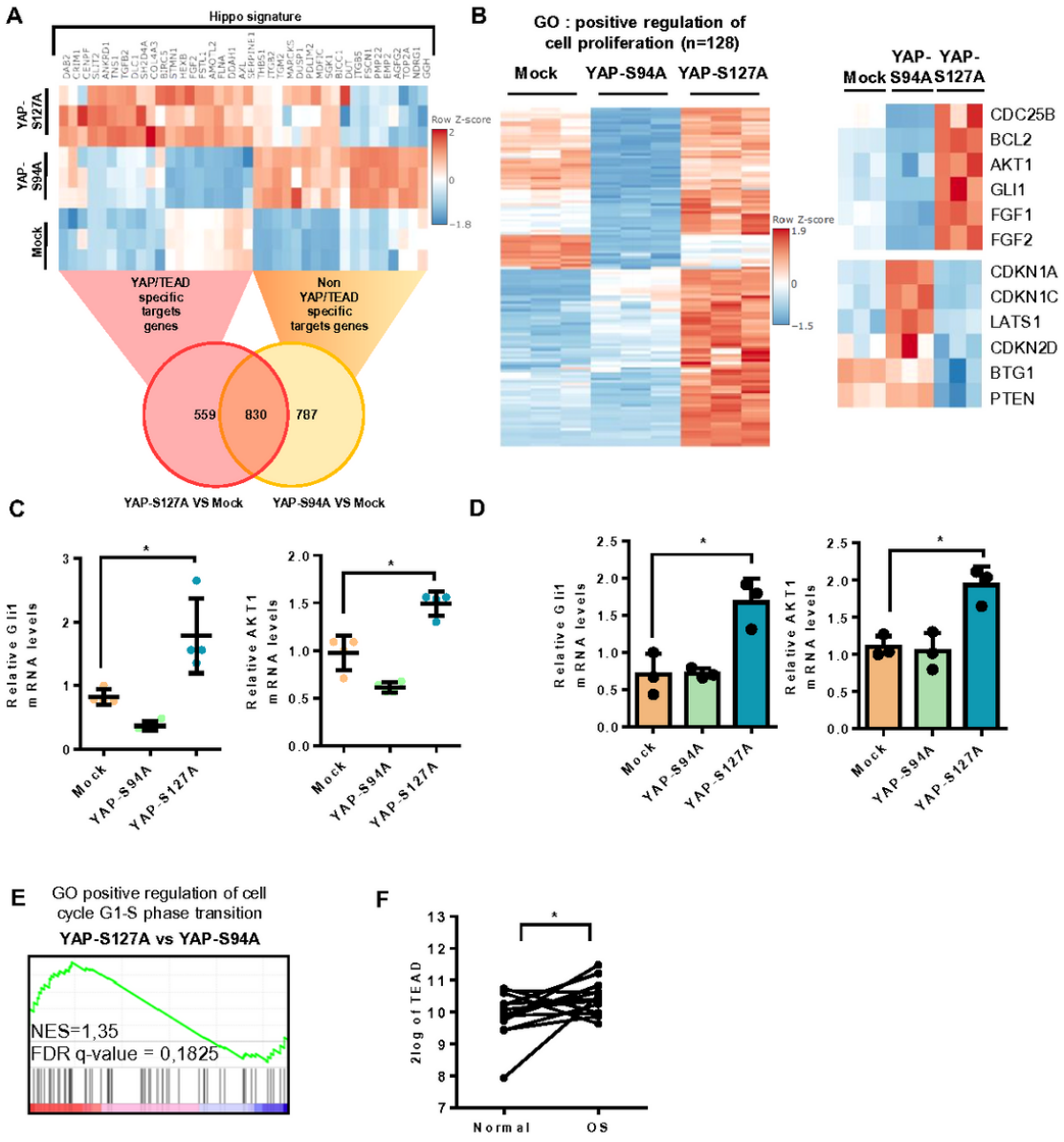

Figure 4

Role of TEAD in YAP-driven cell cycle genes expression A) Heat map of YAP-associated upregulated gene signature in mock-, YAPS94A- and YAPS127A-transfected K-HOS cells. Color scales are based on Z-scores. B) Heat map showing mRNA levels of 128 genes significantly overexpressed in YAPS127A-transfected cells involved in the positive regulation of cell proliferation. Color scales are based on Z-scores. C) Total RNA was extracted from tumor biopsies of mice injected with mock-, YAPS94A- or YAPS127A-transfected cells. Gli1 and AKT1 mRNA steady-state levels were determined by quantitative RT-PCR. Bars indicate means ± S.D. of three independent experiments, each performed in duplicate. (*p<0.05). D) Gli1 and AKT1 mRNA steady-state levels were quantified by RT-qPCR analysis in mock-, YAPS94A- and YAPS127A-transfected K-HOS cells. Bars indicate means ± SD of three independent experiments, each performed in triplicate (*p<0.05). E) Enrichment score (ES) plots of GSEA analysis show a significant upregulation of genes involved in G1-S phase transition in YAPS127A-transfected K-HOS cells compared to YAPS94A-transfected K-HOS cells. F) Relative TEAD1 gene expression in OS patients and control samples of the same patients following bioinformatics analysis of RNAseq data GSE99671 [26] from an OS patient cohort comprising 15 samples.

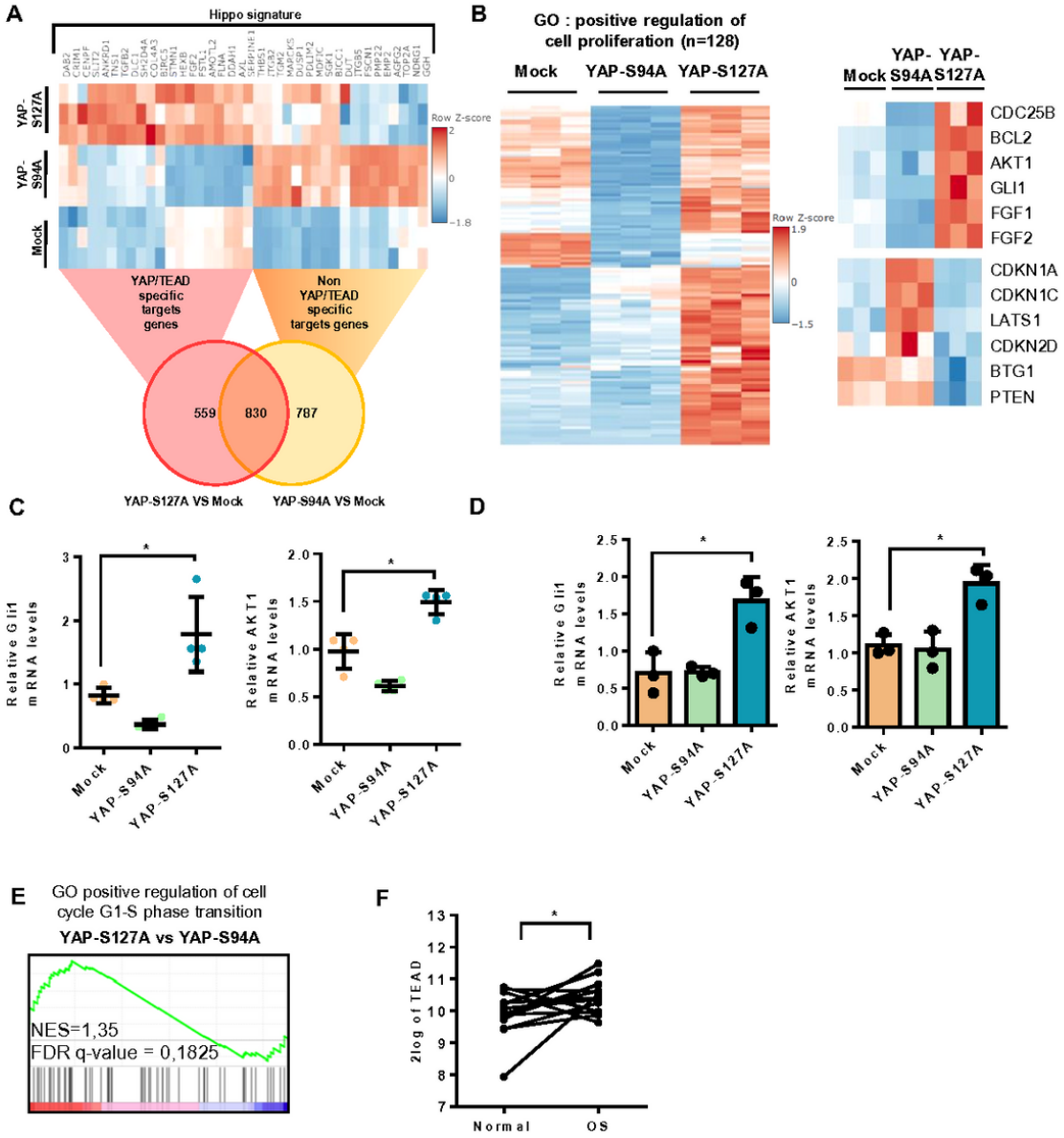

Figure 4

Role of TEAD in YAP-driven cell cycle genes expression A) Heat map of YAP-associated upregulated gene signature in mock-, YAPS94A- and YAPS127A-transfected K-HOS cells. Color scales are based on Z-scores. B) Heat map showing mRNA levels of 128 genes significantly overexpressed in YAPS127A-transfected cells involved in the positive regulation of cell proliferation. Color scales are based on Z-scores. C) Total RNA was extracted from tumor biopsies of mice injected with mock-, YAPS94A- or YAPS127A-transfected cells. Gli1 and AKT1 mRNA steady-state levels were determined by quantitative RT-PCR. Bars indicate means ± S.D. of three independent experiments, each performed in duplicate. (*p<0.05). D) Gli1 and AKT1 mRNA steady-state levels were quantified by RT-qPCR analysis in mock-, YAPS94A- and YAPS127A-transfected K-HOS cells. Bars indicate means ± SD of three independent experiments, each performed in triplicate (*p<0.05). E) Enrichment score (ES) plots of GSEA analysis show a significant upregulation of genes involved in G1-S phase transition in YAPS127A-transfected K-HOS cells compared to YAPS94A-transfected K-HOS cells. F) Relative TEAD1 gene expression in OS patients and control samples of the same patients following bioinformatics analysis of RNAseq data GSE99671 [26] from an OS patient cohort comprising 15 samples.

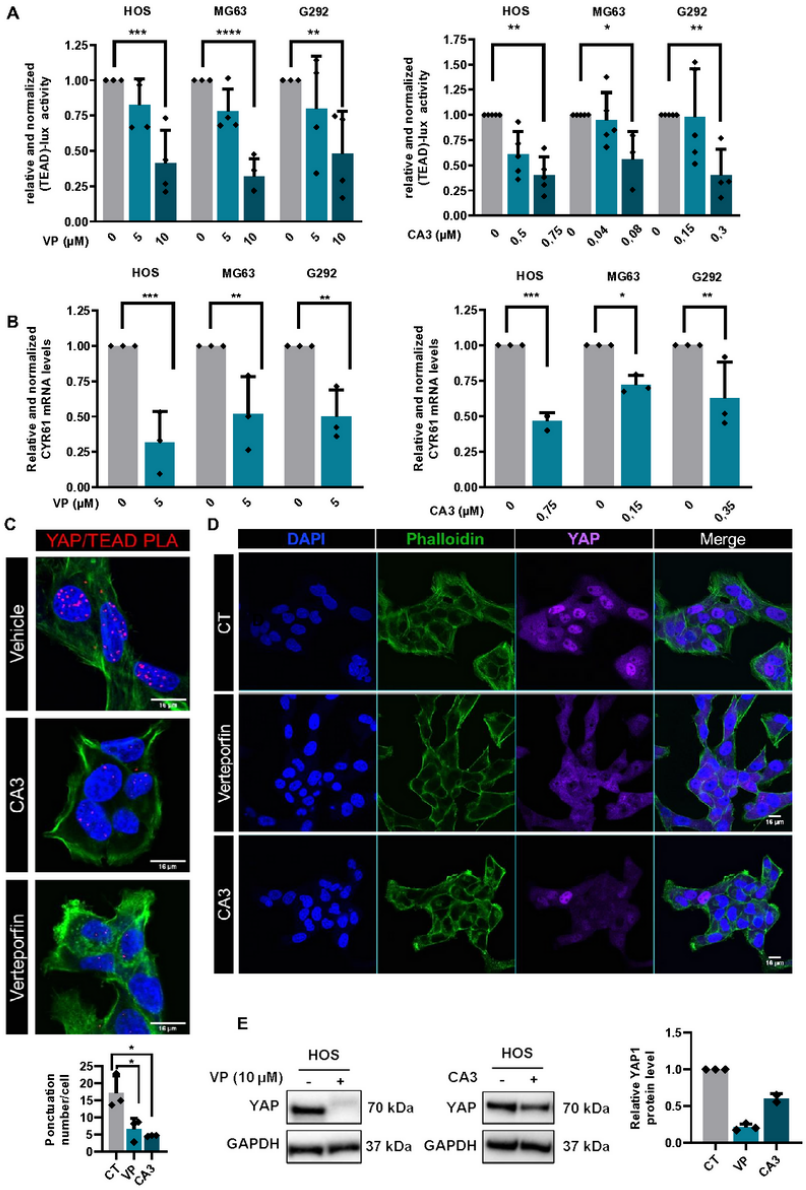

Figure 5

Verteporfin and CA3 inhibit YAP expression and YAP-driven TEAD transcriptional activity A) HOS, MG63 and G292 cells were transfected with the TEAD-specific construct (TEAD)8-lux. 24 h after transfection, cells were treated with verteporfin (left panel) or CA3 (right panel) as indicated concentration for 48 h. Bars indicate means ± S.D. of at least three independent experiments, each performed in duplicate (*p<0.05, **p<0.01, ***P < 0.001, **** < p 0.0001). B) CYR61 mRNA steady-state levels were quantified by RT-q-PCR analysis in the presence or absence of verteporfin (left panel) or CA3 (right panel) 48 h. Bars indicate the means ± SD of three independent experiments, each performed in duplicate (*p<0.05, **p<0.01, ***P < 0.001, **** < p 0.0001). C) Localization of YAP/TEAD1 complexes by in situ PLA experiments in HOS cells treated or not with 10 μM verteporfin and 0.75 μM CA3 during 48 h. The red signal was obtained using Alexa555-labeled hybridization oligo nucleotides targeting amplified in situ PLA products. DAPI (blue) staining was used for nuclear visualization (left panel). Bars indicate means ± S.D. of three independent experiments (**p<0.01, right panel). D) HOS were stimulate or not with 10 μM verteporfin and 0.75 μM CA3 during 48 h and were then fixed, permeabilized and stained with a monoclonal antibody directed against YAP (far-red). F-actin cytoskeleton and nuclei were respectively revealed by phalloidine (green) and DAPI labelling (blue). Photographs representative of two independent experiments are shown. E) YAP production was detected by Western blot analysis in HOS cells treated or not with 10 μM verteporfin and 0.6 μM CA3 during 72 h. Results shown are representative of three independent experiments (right panel).

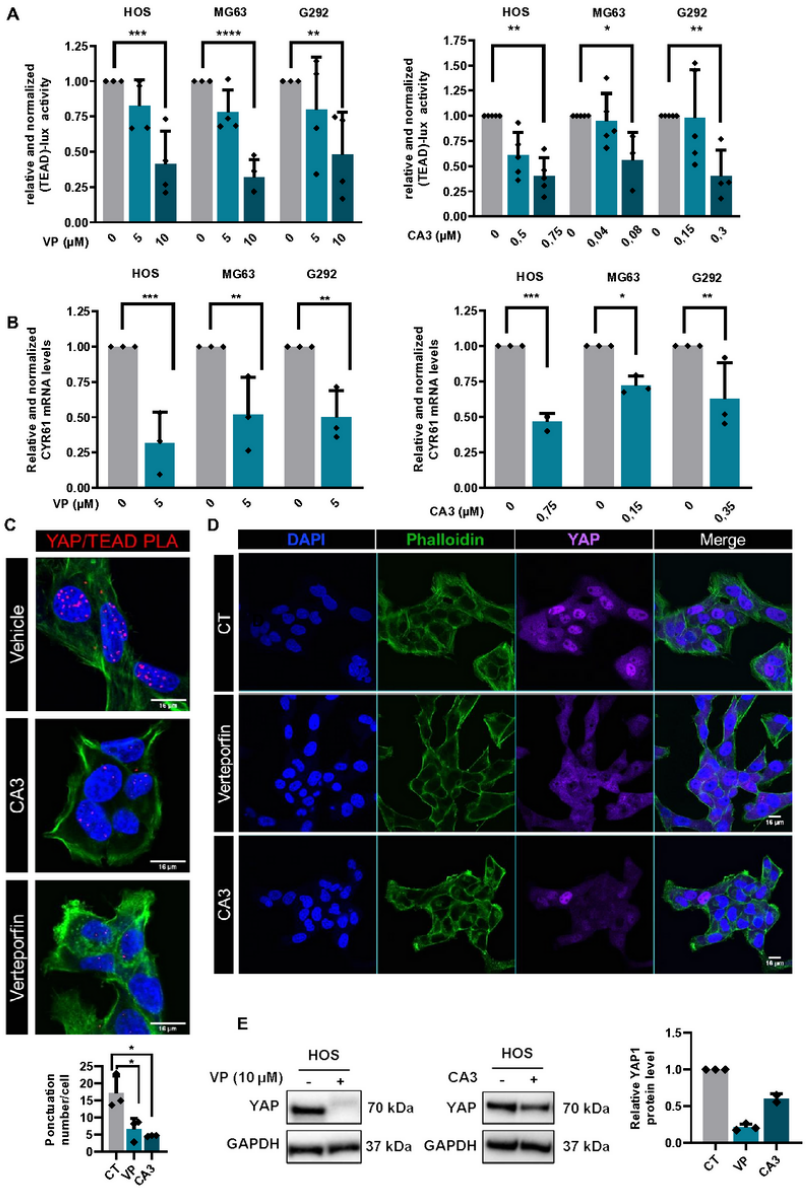

Figure 5

Verteporfin and CA3 inhibit YAP expression and YAP-driven TEAD transcriptional activity A) HOS, MG63 and G292 cells were transfected with the TEAD-specific construct (TEAD)8-lux. 24 h after transfection, cells were treated with verteporfin (left panel) or CA3 (right panel) as indicated concentration for 48 h. Bars indicate means ± S.D. of at least three independent experiments, each performed in duplicate (*p<0.05, **p<0.01, ***P < 0.001, **** < p 0.0001). B) CYR61 mRNA steady-state levels were quantified by RT-q-PCR analysis in the presence or absence of verteporfin (left panel) or CA3 (right panel) 48 h. Bars indicate the means ± SD of three independent experiments, each performed in duplicate (*p<0.05, **p<0.01, ***P < 0.001, **** < p 0.0001). C) Localization of YAP/TEAD1 complexes by in situ PLA experiments in HOS cells treated or not with 10 μM verteporfin and 0.75 μM CA3 during 48 h. The red signal was obtained using Alexa555-labeled hybridization oligo nucleotides targeting amplified in situ PLA products. DAPI (blue) staining was used for nuclear visualization (left panel). Bars indicate means ± S.D. of three independent experiments (**p<0.01, right panel). D) HOS were stimulate or not with 10 μM verteporfin and 0.75 μM CA3 during 48 h and were then fixed, permeabilized and stained with a monoclonal antibody directed against YAP (far-red). F-actin cytoskeleton and nuclei were respectively revealed by phalloidine (green) and DAPI labelling (blue). Photographs representative of two independent experiments are shown. E) YAP production was detected by Western blot analysis in HOS cells treated or not with 10 μM verteporfin and 0.6 μM CA3 during 72 h. Results shown are representative of three independent experiments (right panel).

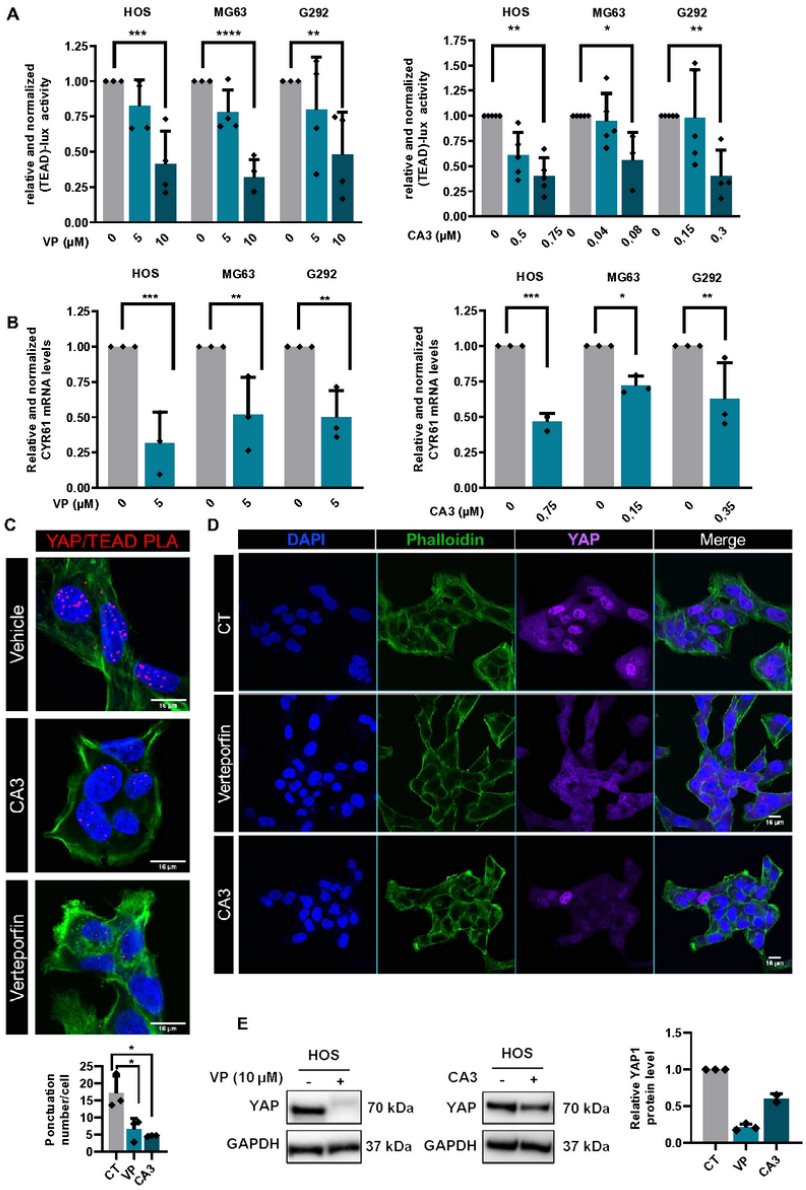

Figure 5

Verteporfin and CA3 inhibit YAP expression and YAP-driven TEAD transcriptional activity A) HOS, MG63 and G292 cells were transfected with the TEAD-specific construct (TEAD)8-lux. 24 h after transfection, cells were treated with verteporfin (left panel) or CA3 (right panel) as indicated concentration for 48 h. Bars indicate means ± S.D. of at least three independent experiments, each performed in duplicate (*p<0.05, **p<0.01, ***P < 0.001, **** < p 0.0001). B) CYR61 mRNA steady-state levels were quantified by RT-q-PCR analysis in the presence or absence of verteporfin (left panel) or CA3 (right panel) 48 h. Bars indicate the means ± SD of three independent experiments, each performed in duplicate (*p<0.05, **p<0.01, ***P < 0.001, **** < p 0.0001). C) Localization of YAP/TEAD1 complexes by in situ PLA experiments in HOS cells treated or not with 10 μM verteporfin and 0.75 μM CA3 during 48 h. The red signal was obtained using Alexa555-labeled hybridization oligo nucleotides targeting amplified in situ PLA products. DAPI (blue) staining was used for nuclear visualization (left panel). Bars indicate means ± S.D. of three independent experiments (**p<0.01, right panel). D) HOS were stimulate or not with 10 μM verteporfin and 0.75 μM CA3 during 48 h and were then fixed, permeabilized and stained with a monoclonal antibody directed against YAP (far-red). F-actin cytoskeleton and nuclei were respectively revealed by phalloidine (green) and DAPI labelling (blue). Photographs representative of two independent experiments are shown. E) YAP production was detected by Western blot analysis in HOS cells treated or not with 10 μM verteporfin and 0.6 μM CA3 during 72 h. Results shown are representative of three independent experiments (right panel).

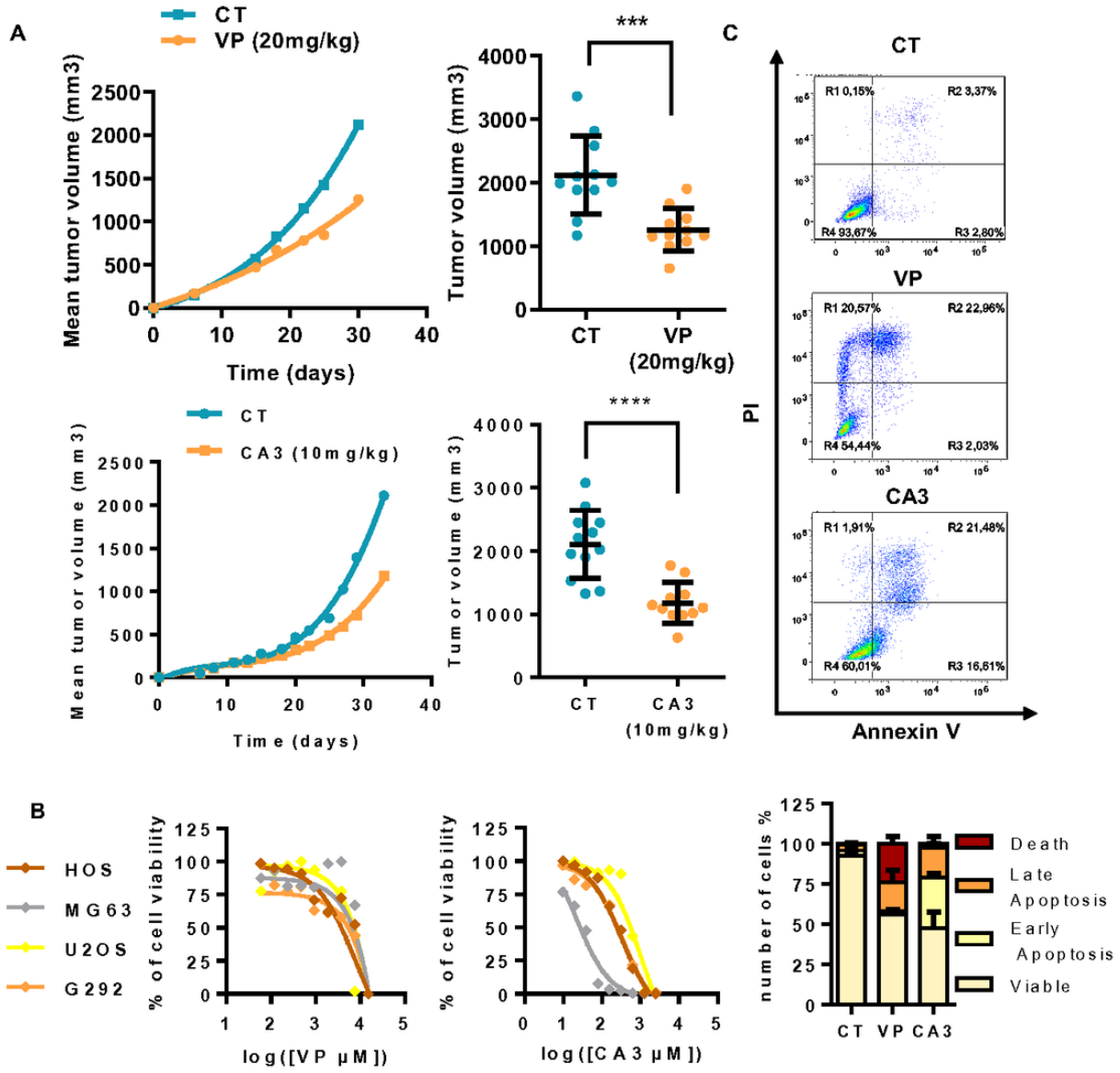

Figure 6

CA3 inhibits OS primary bone tumor growth A) Intramuscular paratibial injections of 1.106 HOS cells were performed in two groups of 12 nude mice treated with vehicle or verteporfin (20 mg/kg), and vehicle or CA3 (10 mg/kg) as indicated. Tumor volumes were measured three times per week for 4 weeks. Means tumor volumes of each group were measured 30 or 33 days after cell injection (right panels, mean ± SD; ***p < 0.001, ****p<0.0001). B) HOS, MG63, and G292 OS cell lines were treated with verteporfin (left panel) or CA3 (right panel) as indicated for 72 h. Graph represent cell viability after treatment. Mean of three independent experiments, each performed in sextuplicate. C) Upper panels: Representative dot plots of HOS cells untreated or treated with 10 µM verteporfin or 0.75 µM CA3 for 72 h are shown (representative graphs of three experiments). Lower panels: Bars indicate the means ± SD of the relative number of lives cells, death cells, and cells in early- or late-phase apoptosis (n = 3 independent experiments).

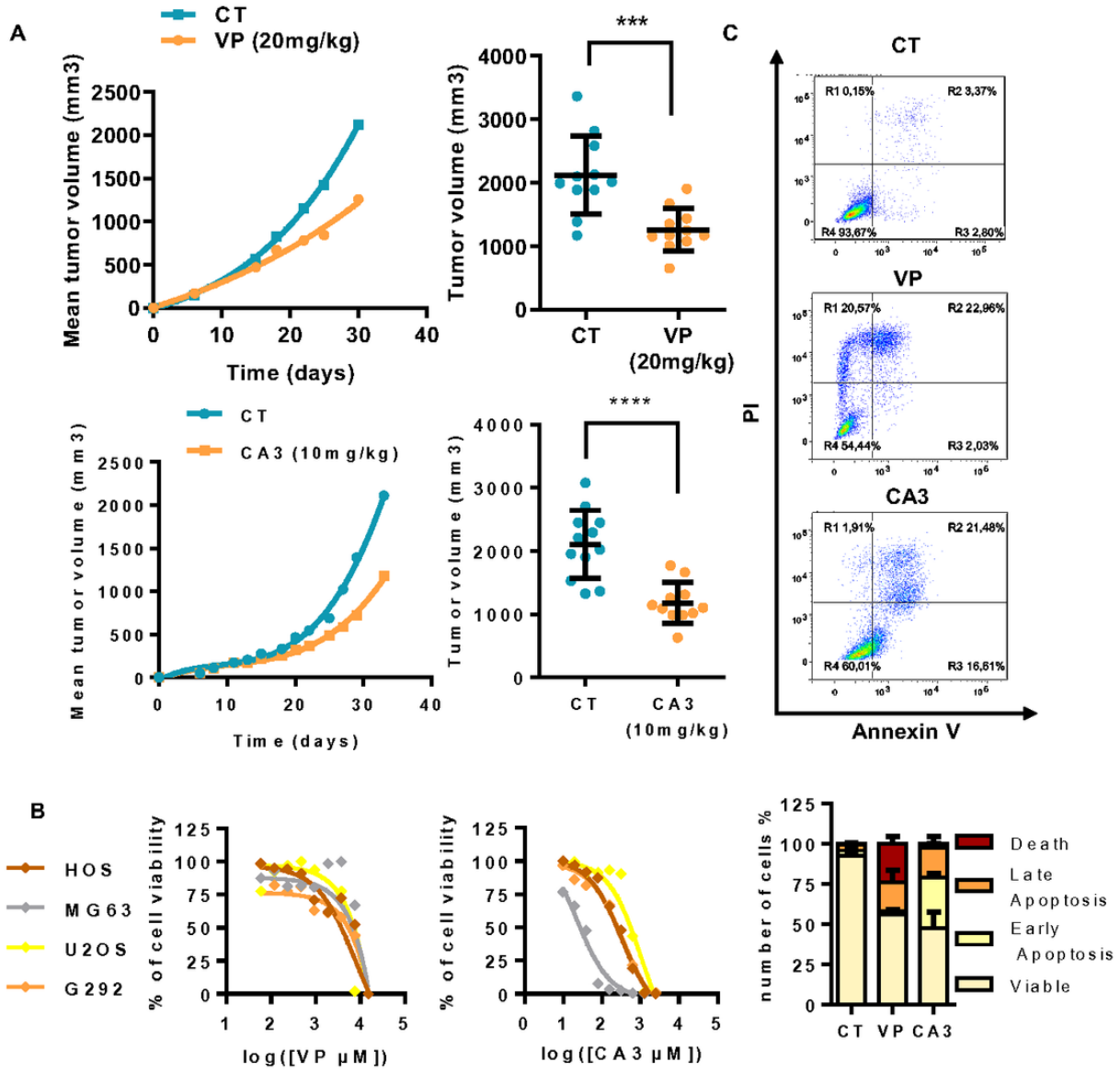

Figure 6

CA3 inhibits OS primary bone tumor growth A) Intramuscular paratibial injections of 1.106 HOS cells were performed in two groups of 12 nude mice treated with vehicle or verteporfin (20 mg/kg), and vehicle or CA3 (10 mg/kg) as indicated. Tumor volumes were measured three times per week for 4 weeks. Means tumor volumes of each group were measured 30 or 33 days after cell injection (right panels, mean ± SD; ***p < 0.001, ****p<0.0001). B) HOS, MG63, and G292 OS cell lines were treated with verteporfin (left panel) or CA3 (right panel) as indicated for 72 h. Graph represent cell viability after treatment. Mean of three independent experiments, each performed in sextuplicate. C) Upper panels: Representative dot plots of HOS cells untreated or treated with 10 µM verteporfin or 0.75 µM CA3 for 72 h are shown (representative graphs of three experiments). Lower panels: Bars indicate the means ± SD of the relative number of lives cells, death cells, and cells in early- or late-phase apoptosis (n = 3 independent experiments).

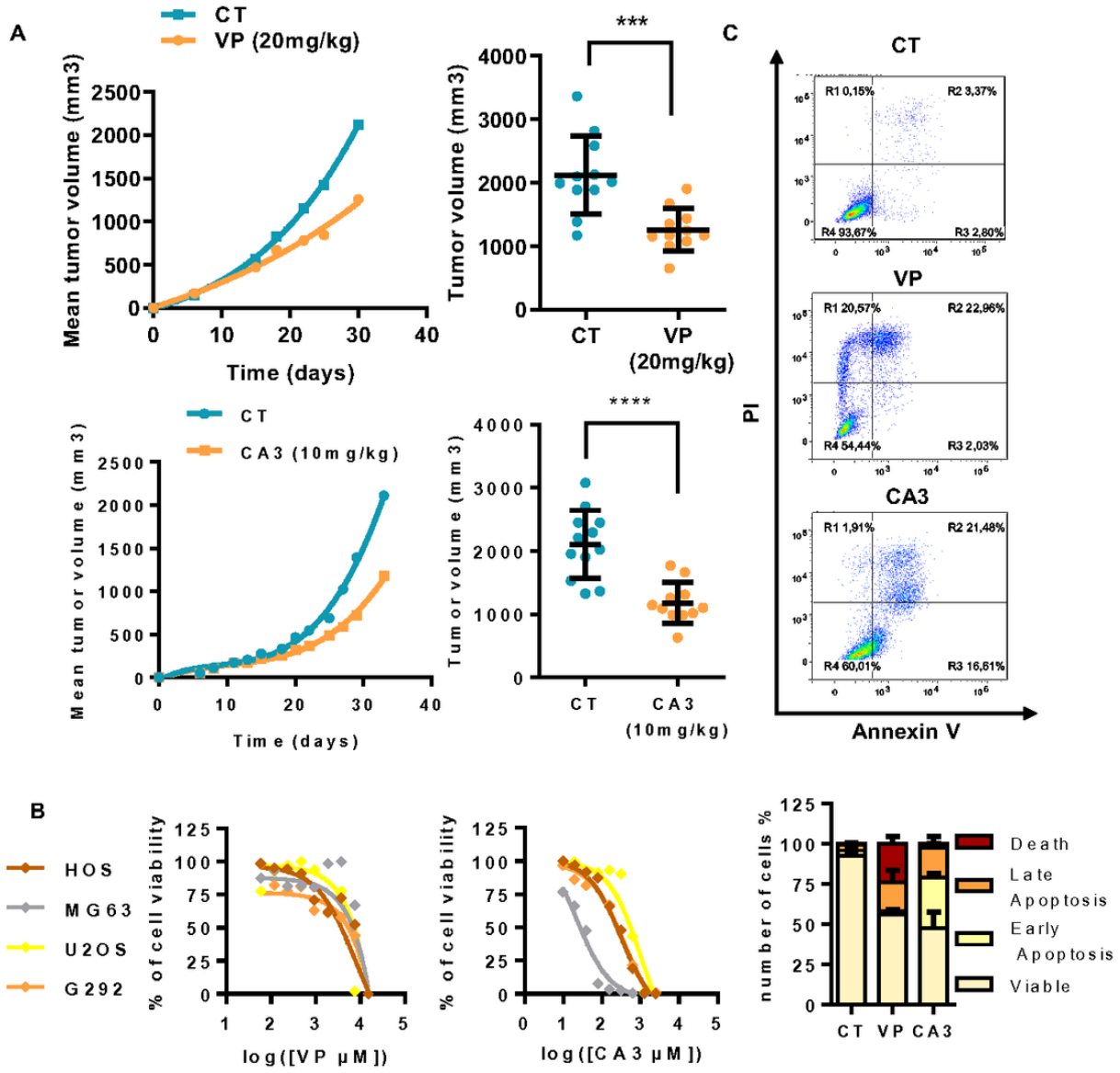

Figure 6

CA3 inhibits OS primary bone tumor growth A) Intramuscular paratibial injections of 1.106 HOS cells were performed in two groups of 12 nude mice treated with vehicle or verteporfin (20 mg/kg), and vehicle or CA3 (10 mg/kg) as indicated. Tumor volumes were measured three times per week for 4 weeks. Means tumor volumes of each group were measured 30 or 33 days after cell injection (right panels, mean ± SD; ***p < 0.001, ****p<0.0001). B) HOS, MG63, and G292 OS cell lines were treated with verteporfin (left panel) or CA3 (right panel) as indicated for 72 h. Graph represent cell viability after treatment. Mean of three independent experiments, each performed in sextuplicate. C) Upper panels: Representative dot plots of HOS cells untreated or treated with 10 µM verteporfin or 0.75 µM CA3 for 72 h are shown (representative graphs of three experiments). Lower panels: Bars indicate the means ± SD of the relative number of lives cells, death cells, and cells in early- or late-phase apoptosis (n = 3 independent experiments).

Supplementary Files

This is a list of supplementary files associated with this preprint. Click to download.

- MoriceetalAdditionalfiles.docx
- MoriceetalAdditionalfiles.docx
- MoriceetalAdditionalfiles.docx